

Review

# Nano-Structured Dilute Magnetic Semiconductors for Efficient Spintronics at Room Temperature

Akanksha Gupta <sup>1</sup>, Rui Zhang <sup>2</sup>, Pramod Kumar <sup>3</sup>, Vinod Kumar <sup>4,5,\*</sup>  and Anup Kumar <sup>6,\*</sup>

<sup>1</sup> Department of Chemistry, Sri Venkateswara College, University of Delhi, Delhi 110021, India; akankshachem05@gmail.com

<sup>2</sup> MOE Key Laboratory for Nonequilibrium Synthesis and Modulation of Condensed Matter, State Key Laboratory for Mechanical Behavior of Materials, Xi'an Jiaotong University, Xi'an 710049, China; RUZHANG@tcd.ie

<sup>3</sup> Department of Chemistry, Sri Aurobindo College, University of Delhi, Delhi 110017, India; nita\_pramod@yahoo.com

<sup>4</sup> Department of Chemistry, Kirori Mal College, University of Delhi, Delhi 110007, India

<sup>5</sup> Special Centre for Nano Sciences, Jawaharlal Nehru University, Delhi 110067, India

<sup>6</sup> School of Physics, Trinity College, Dublin D02 PN40, Ireland

\* Correspondence: vinodkumar@kmc.du.ac.in (V.K.); ankumar@tcd.ie (A.K.)

Received: 20 September 2019; Accepted: 14 February 2020; Published: 16 March 2020



**Abstract:** In recent years, many efforts have been made to develop advanced metal oxide semiconductor nanomaterials with exotic magnetic properties for modern applications w.r.t traditional analogues. Dilute magnetic semiconductor oxides (DMSOs) are promising candidates for superior control over the charge and spin degrees of freedom. DMSOs are transparent, wide band gap materials with induced ferromagnetism in doping, with a minor percentage of magnetic *3d* cation to create a long-range antiferromagnetic order. Although significant efforts have been carried out to achieve DMSO with ferromagnetic properties above room temperature, it is a great challenge that still exists. However, TiO<sub>2</sub>, SnO<sub>2</sub>, ZnO and In<sub>2</sub>O<sub>3</sub> with wide band gaps of 3.2, 3.6, 3.2 and 2.92 eV, respectively, can host a broad range of dopants to generate various compositions. Interestingly, a reduction in the size of these binary oxides can induce ferromagnetism, even at room temperature, due to the grain boundary, presence of defects and oxygen vacancies. The present review provides a panorama of the structural analysis and magnetic properties of DMSOs based on binary metal oxides nanomaterials with various ferromagnetic or paramagnetic dopants, e.g., Co, V, Fe and Ni, which exhibit enhanced ferromagnetic behaviors at room temperature.

**Keywords:** TiO<sub>2</sub>; SnO<sub>2</sub>; ZnO; In<sub>2</sub>O<sub>3</sub>; ferromagnetic

## 1. Introduction

Persistent efforts to achieve substantially smaller information storage devices open up many areas of interest for research, alongside certain challenges. In this regard, spintronics offers the utilization of electron spin and charge to enhance information density. The development of functional ferromagnetic semiconductors at room temperature, i.e., the combination of the functionality of semiconductors and ferromagnets, is the goal of spin-based electronics. In this way, interest in dilute magnetic semiconductors (DMSs), mainly dilute magnetic oxides (DMOs) or dilute magnetic semiconductor oxides (DMSOs), has been rapidly increasing due to their potential application in spintronics devices. Low-temperature ferromagnetism in (Ga,Mn)As, *p*-(Cd,Mn)Te and similar compositions, and calculations on doped, nitride and oxide semiconductors which might be able to explain the ferromagnetism via valence-band holes at lower temperatures, have been much sought-after areas in magnetism research [1]. At a low concentration of donors, the localized impurity band forms,

but above critical concentration, and the delocalized effects and spontaneous magnetic ordering in  $d^0$  ferromagnetism (FM), in a series of doped wide band gap oxides remain areas of debate [2,3]. In this way, the usual magnetic signatures of DMS and DMSO are attributed due to transition metal (TM) impurities and their hybridization with non-TM neighbors. However, long-range ferromagnetic ordering can be induced via a number of causes, such as ion vacancies, F centers, dangling bonds, unpaired electrons are residing in crystallites, intercrystalline grains, or at the surface/interfaces [4]. Coey et al. discussed ferromagnetic exchange coupling in DMSOs through simple model where shallow donor electrons (e.g., oxygen vacancy) form magnetic polarons that mediate magnetic ordering in these materials. Curie temperatures higher than 300 K, with significant magnetic moments, per transition metal cation in dilute ferromagnetic oxides, make it difficult to understand the magnetism in these solids. These materials have high- $k$  dielectrics and thermally activated  $n$ -type semiconductivity [5]. It is crucial to generate such multifunctional materials in the modern world, and DMS could be used to accomplish the criteria. DMS can be formed by adding magnetic impurities at very low concentrations to the host lattice, without changing the lattice that emerged from the resulting materials, for lots of modern devices, e.g., next-generation spintronics-based multifunctional devices, because of the existence of ferromagnetism above room temperature [5,6].

Matsumoto et al. demonstrated significant ferromagnetism (0.32 Bohr magnetons/cobalt atom) in Co:TiO<sub>2</sub> thin films due to long range ferromagnetism ordering [7]. Interestingly, an electric field tunable magnetic moment was executed by (Ti,Co)O<sub>2</sub>, at room temperature with electrochemical high-density electron double-layer gating and the application of a gate voltage to transform the low carrier density paramagnetic state into a high carrier density ferromagnetic state, which could play a significant part in ferromagnetism above room temperature for viable commercial spintronics [8].

The intrinsic ferromagnetism in Co:TiO<sub>2</sub>, induced by oxygen vacancies, has been reported by Saadaoui et al. [9]. Similarly, Nd-doped ZnO nanowires show ferromagnetic properties above room temperature with a saturation magnetic moment of 4.1  $\mu\text{B}/\text{Nd}$  and remarkable coercivity of 780 Oe, with high magnetic anisotropy. This intrinsic magnetism resulted from the density of defects [10]. Moreover, a giant coercivity of 1200 Oe at ambient temperature was reached by cluster-free co-doping with Co and Eu [11]. Transparent Co-doped SnO<sub>2</sub> showed high temperature ferromagnetism with a giant magnetic moment of  $7.5 \pm 0.5 \mu\text{B}/\text{Co}$ , with no Co clustering [12]. In this review, we have focused on four basic binary oxide semiconductors, TiO<sub>2</sub>, SnO<sub>2</sub>, ZnO and In<sub>2</sub>O<sub>3</sub> and their ferromagnetic properties.

SnO<sub>2</sub> exhibits a rutile structure, TiO<sub>2</sub> has both a rutile and anatase form. Hexagonal ZnO has a wurtzite structure (direct energy band gap, 3.37 eV) with a lattice parameter of  $c/a = 1.633$  and  $P6_3mc$  space group (Figure 1). The rutile structures of SnO<sub>2</sub> and TiO<sub>2</sub> possess tetragonal symmetry, crystallizing in the  $P4_2/mnm$  space group, with  $a = 4.755 \text{ \AA}$ ,  $c = 3.199 \text{ \AA}$  (SnO<sub>2</sub>) and  $a = 4.592 \text{ \AA}$ ,  $c = 2.957 \text{ \AA}$  (TiO<sub>2</sub>). In SnO<sub>2</sub> and TiO<sub>2</sub>, the octahedral coordination around the anion is slightly distorted and the valence bands of SnO<sub>2</sub> contain a mixture of the O2 $p$  orbital within 5 $s$  and 5 $p$ , whereas the 5 $s$  orbital contributes, chiefly, to the conduction band. In addition, TiO<sub>2</sub> has a similar structure to SnO<sub>2</sub>, which comprises Ti 3 $d$  and the O 2 $p$  orbitals near the Fermi level, where the upper valence band is governed by the O 2 $p$  orbitals and the conduction band by Ti 3 $d$  states [13]. In<sub>2</sub>O<sub>3</sub> exhibits a cubic bixbyite crystal structure with an S.G.  $Ia\bar{3}$ , lattice dimension  $a = 10.117 \text{ \AA}$  and a band gap of 3 eV (Figure 1). TiO<sub>2</sub> electrodes exhibit superior cycling stability and coulombic efficiency and a low reversible capacity w.r.t. other transition oxides. Transition metal oxide-based electrodes reveal an enhanced irreversible capacity and a lower coulombic efficiency [14]. Similarly, SnO<sub>2</sub>- and ZnO-based electrodes are viable for lithium ion batteries, transparent conducting oxides, photoelectrochemical properties, etc. [15,16].

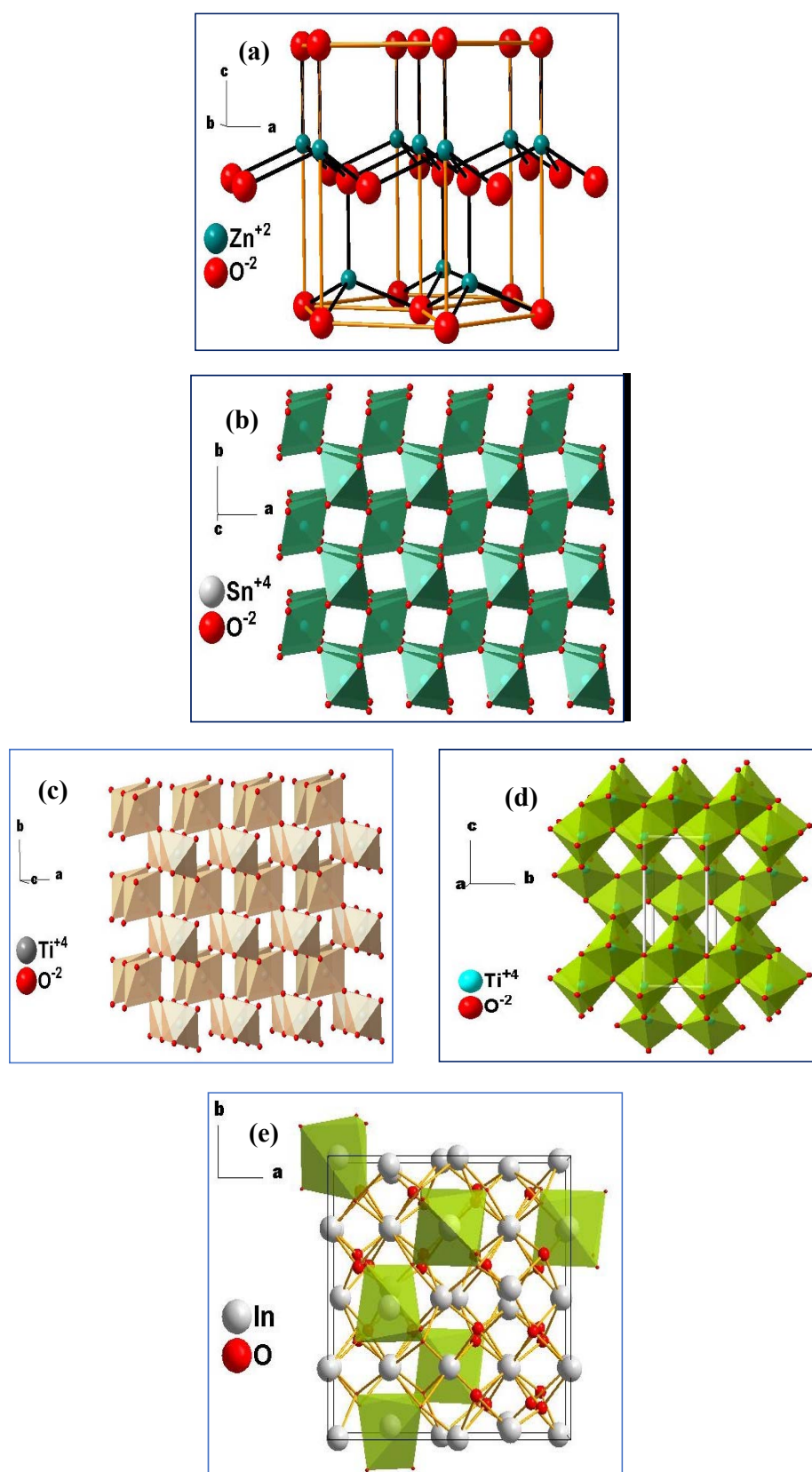


**Figure 1.** Crystal structures of (a) ZnO (wurtzite), (b) SnO<sub>2</sub> (rutile), (c) TiO<sub>2</sub> (rutile), (d) TiO<sub>2</sub> (anatase) and (e) In<sub>2</sub>O<sub>3</sub> (bixbyite).

Magnetite has a cubic inverse spinel crystal structure with space group  $Fd\bar{3}m$  and has revealed electric and magnetic behavior via electron exchange in a mixed valence  $Fe^{2+}/Fe^{3+}$  state, leading potential uses in catalysis, magnetic recording, ferro fluids, clinical diagnosis, etc. Additionally, monodispersed nanocrystals with suitable sizes/size distribution could add additional functionality to scientific and technological interests. Alloys based on iron/magnetite were unsuitable due to eddy-current losses [17–20]. Magnetite shows the ferrimagnetic properties associated with congruent spins that are partially oriented in their field direction. However, the magnetic domains in magnetite-independent moment vectors display definite magnitudes and directions [21]. Importantly, the transformation of multi-domains to a single-domain state for ferromagnetic materials is possible via particle-size engineering [22–24].

However, binary oxides  $TiO_2$ ,  $SnO_2$ ,  $ZnO$  and  $In_2O_3$  are intrinsically diamagnetic, while the grain boundary, presence of defects and oxygen vacancies produced in the nano regime induce the unexplainable magnetism at room temperature (RT) [25,26]. These nanomaterials can be used in spintronics applications in place of magnetite.

## 2. Theory of Ferromagnetism in Oxides

The mechanism responsible for initiating room temperature ferromagnetism (RTFM) can be introduced in non-magnetic semiconductors (NMSs) through charge and spin of electrons as explained in Figure 2. If the number of magnetic elements are more, then it may cause ferromagnetism (Figure 2b), however, DMS may be achieved on introducing few magnetic elements into NMSs (Figure 2c) due to inducing spin-polarization in crystal lattice originate from dopant lattices.

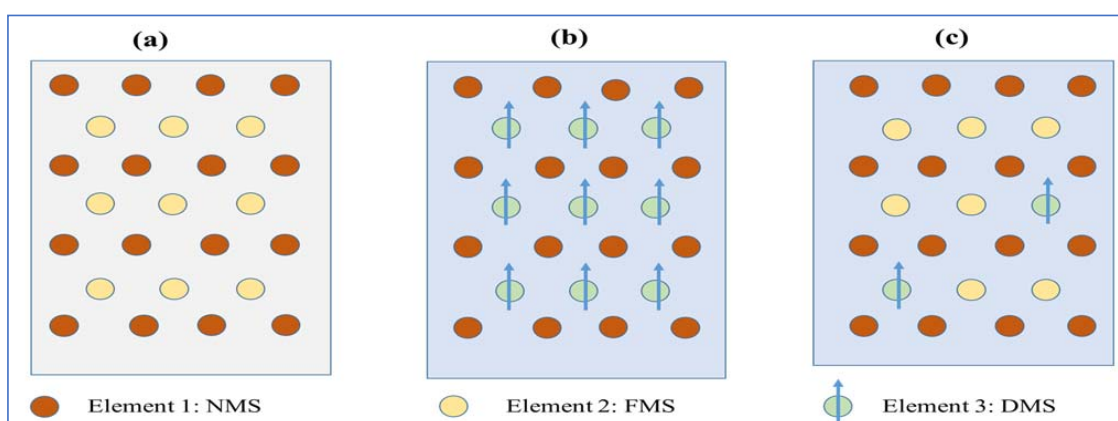


**Figure 2.** Three types of semiconductors: (a) Non-magnetic semiconductor (NMS), (b) ferromagnetic semiconductor (FMS): addition of magnetic transition metal ions in a non-magnetic semiconductor where arrows represent domain with orientated spin polarization and (c) dilute magnetic semiconductor on introduction of a small fraction of magnetic transition metal ions.

A schematic representation of FM in  $Co:TiO_2$  is shown in Figure 3. Titanium  $3d$  electrons travel around the material aligning the spin of cobalt atoms to point in the same direction [27]. Using various TM ions, dopants perturb the semiconductor oxides in two ways. In the first one, if dopants substitute at metal ion site will strongly perturb conduction band and therefore, reduce the mobility of electrons by dispersion of the electrons [28]. In another case, if dopants available at oxygen lattice, then it will perturb the valence band hence obtain higher mobility of electrons due to the conduction band free from dispersion. Furthermore, due to different ionic sizes and charges of dopants, distortion occur in the structure in several ways as shown in Figure 4 [29]. Hence, an appropriate selection of the dopants for metal oxide semiconductors is significant for acquiring better quality spintronics materials. A consideration of this paradox is vital to determine the type of electrons or charge carriers that mediate the ferromagnetism in a material to design efficient spintronic devices.

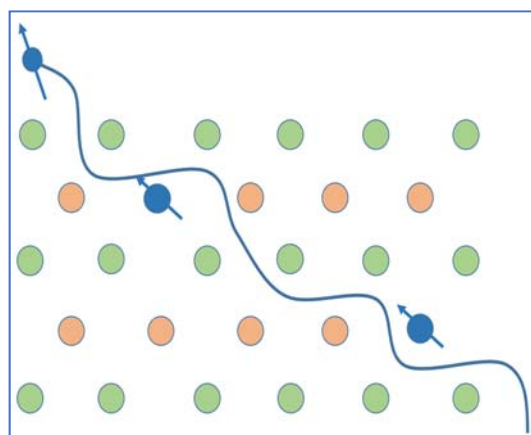


**Figure 3.** A schematic representation of ferromagnetism in Co:TiO<sub>2</sub>. The orange, green and blue spheres correspond to titanium, oxygen and cobalt atoms, respectively [27].

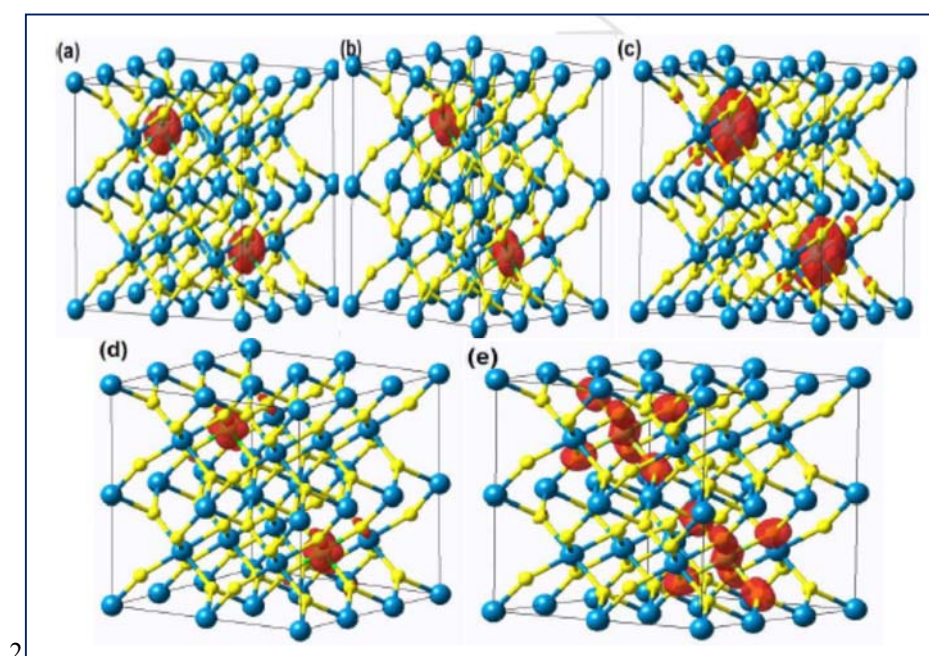


**Figure 4.** Comparative diagram for local magnetization density for (a) Mn, (b) Fe, (c) Cr, (d) Co and (e) Zn doped SnO<sub>2</sub> (The Figure is reproduced by copyright permission from reference [29]).

It is well known that the magnetic properties in doped nanomaterials such as metal oxides, and superparamagnetic iron oxide, chalcogenide semiconductors [30,31] are dependent on nature and extent of doping along with synthesis characteristic. Incorporation of several transition metal dopant in host ranging from ZnO, SnO<sub>2</sub>, TiO<sub>2</sub>, etc. develop DMS material possessing different surface properties and size of materials etc. [32] from the various synthesis protocol and even saturated magnetic moment can be enhanced by annealing at a suitable temperature [33].

### 3. TiO<sub>2</sub> and Ferromagnetism

TiO<sub>2</sub> is the well-known and widely used semiconductor having both rutile and anatase structure (Figure 1) with a wide bandgap that can be engineered easily on doping and also, various properties can be modified easily such as optical, electrical as well as magnetic properties. Choudhary et al. examined the effect of Mn on TiO<sub>2</sub> nanoparticles formed by a sol-gel method of size range 6–11 nm displayed magnetic properties at room and low temperature. The mechanism of paramagnetism

and antiferromagnetism is shown in Figure 5 [33].  $\text{Mn}^{2+}$  magnetic spins and exchange interaction of  $\text{Mn}^{2+}$ – $\text{Mn}^{2+}$  are responsible for paramagnetic behavior whereas negative Curie–Weiss temperature showed antiferromagnetic interaction of  $\text{Mn}^{2+}$  ions through lattice oxygen (Figure 5) [34]. Sharma et al. reported Mn-doped  $\text{TiO}_2$  thin films on quartz by spray pyrolysis and investigated RTFM due to bound magnetic polarons (BMP) [35]. A stable anatase phase, Ni-doped  $\text{TiO}_2$  nanocrystals synthesized by sol-gel technique with different concentration of Ni, coercivity decreases on Ni addition and magnetic properties were observed because of oxygen vacancies and bound magnetic polarons (BMP) (Figure 6). The defects confirmed by PL analysis and Langevin fitting used to determine the concentration of BMPs arising. The higher magnetic moment found in Ni-doped  $\text{TiO}_2$  revealed to show applications in magneto-optics and spintronics [36]. Hou et al. synthesized Ni-doped anatase  $\text{TiO}_2$  thin film by reactive magnetron sputtering on silica substrate. He investigated the effect of Ni-doped on RTFM which shows high correlation between oxygen vacancies [37].

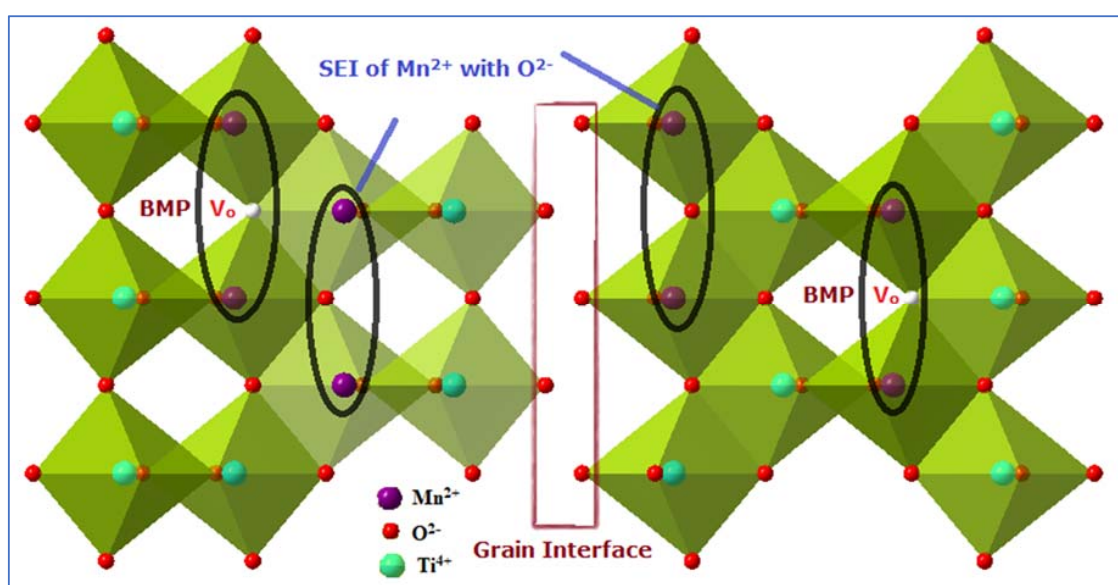


**Figure 5.** Schematic depicting two grains of Mn-doped  $\text{TiO}_2$  (anatase) separated by grain boundary with bound magnetic polarons (BMP) among  $\text{Mn}^{2+}$ – $\text{V}_o$ – $\text{Mn}^{2+}$  and superexchange interactions (SEI) of  $\text{Mn}^{2+}$  with  $\text{O}^{2-}$ .

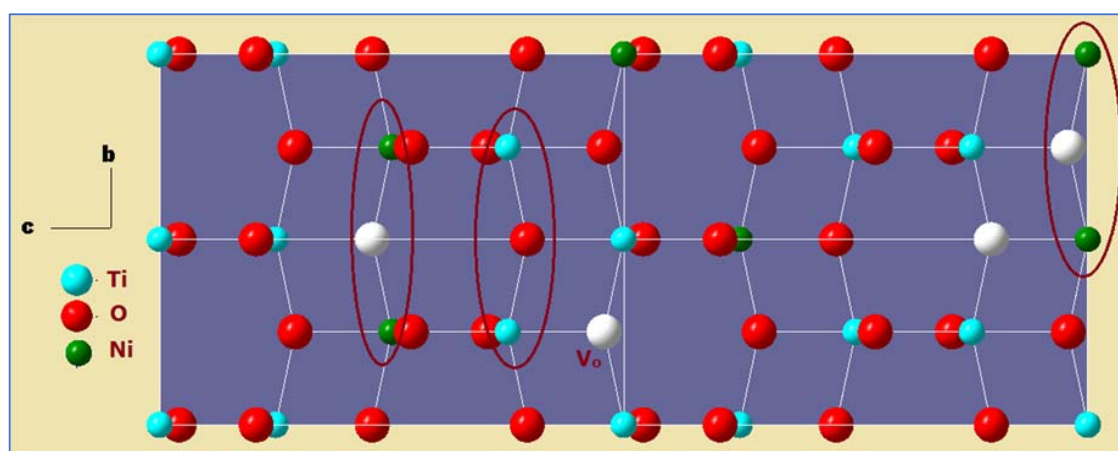


**Figure 6.** Bound magnetic polarons mechanism in Ni doped  $\text{TiO}_2$ .

Rodríguez et al. synthesized nanoparticles of Fe doped  $\text{TiO}_2$  anatase phase by a microemulsion method and the X-ray absorption technique confirmed the presence of  $\text{Fe}^{3+}$  at  $\text{Ti}^{4+}$  site in the  $\text{TiO}_2$

system. Using the Mossbauer and magnetic measurements, he observed that electronic defects also affect the ferromagnetic ordering along with oxygen defects and magnetic ions [38]. Chen et al. showed that oxygen vacancies increase the FM in the rutile structured Fe doped TiO<sub>2</sub> through DFT calculations. More profound defects due to oxygen vacancies or trapping of electrons by Fe atom origin of DMS [39]. Santara et al. synthesized Fe doped TiO<sub>2</sub> nanoribbons mixed-phase rutile and anatase by solvothermal method and observed strong RTFM because of oxygen vacancies and Fe content. RTFM reduction with Fe concentration due to superexchange interaction was mentioned in the report. In addition, it was found that a decrease in FM with increase in annealing temperature for 0.1% Fe doped TiO<sub>2</sub> due to migration of Ti<sup>3+</sup> towards the surface and oxidized to Ti<sup>4+</sup> which reduce the BMPs while highest magnetization (*M<sub>s</sub>*) was observed on vacuum-annealing the same nanomaterials [40]. Fajariah et al. predicted FM in TiO<sub>2</sub> when various TM ions were introduced using DFT calculations [41]. Zero magnetic moments generated by Sc and Ni ions while maximum magnetism was observed in Fe and Mn. Rutile phased Fe doped TiO<sub>2</sub> was explored by Mallia et al. using hybrid-exchange DFT for DMS [42]. It was noted that oxygen stoichiometry and the presence of Fe in the TiO<sub>2</sub> lattice mainly affects ferromagnetism. Bapna et al. investigated the anatase form of Fe (4–8 at.%) doped TiO<sub>2</sub> thin film grown on silicon substrate by PLD technique for RTFM [43]. Ti<sup>3+</sup> defect state, oxygen vacancies and electronic structure are the main factors for RTFM. Ogale et al. explored the room temperature FM in Co-doped TiO<sub>2</sub> thin film [44]. Uniform distribution of Co and tiny Co cluster through the film cross-section driven the FM. Rutile structured Co:TiO<sub>2</sub> thin film fabricated by laser molecular beam epitaxy. Enormous generated oxygen vacancies and high spin Co<sup>2+</sup> ions cause charge imbalance and lattice distortion along with high charge carriers that favors high-temperature FM [45]. Song et al. investigated the effect of 6% Ga and Al as dopants on rutile TiO<sub>2</sub> thin film on Al<sub>2</sub>O<sub>3</sub> by PLD [46]. Magnetic polaron model explained the ferromagnetism behavior in Ga doped TiO<sub>2</sub> that higher the oxygen vacancies, more the Ti<sup>3+</sup> ions responsible for the ferromagnetism and antiferromagnetism coupling with high magnetic moment and T<sub>c</sub>. Zhu et al. grew defective anatase TiO<sub>2</sub> (001) facet on reduced graphene oxide (rGO) and investigated dilute RTFM behavior through the healing effect of rGO [47]. Two different types oxygen vacancies defects on surface and at subsurface was explored using first principle simulations where oxygen vacancies at subsurface attribute significant amount of FM. It also demonstrated that healing effect due to functional group of rGO removed oxygen defects at surface which cause better interface and interaction with oxygen vacancies at subsurface enhanced the same. Some of the recent reports are summarized in Table 1.

**Table 1.** Reports on magnetism data on TiO<sub>2</sub> with various dopants.

Materials	Dopants %	Temp.	Reason for Magnetism	Value of Magnetism	Ref.
TiO <sub>2</sub>		RT	Oxygen vacancies		[25]
Mn doped TiO <sub>2</sub>	10, 15%	RT	Bound magnetic polarons	0.035, 0.017 μ <sub>B</sub> /Mn	[35]
Anatase Ni doped TiO <sub>2</sub>	3, 6, 9, 12 mol.%	RT	BMP, oxygen vacancy, Ti interstitial defects	7.21–11.33 × 10 <sup>-3</sup> μ <sub>B</sub>	[36]
Ni doped TiO <sub>2</sub>	2, 4, 6, 8 mol.%	RT	Oxygen vacancies	0.61, 0.79, 0.89, 1.0 μ <sub>B</sub> /Ni	[37]
Anatase Fe doped TiO <sub>2</sub>	2.8, 5.4%	RT	Fe, oxygen vacancy, other electronic defects	4.7, 4.5 μ <sub>B</sub>	[38]
Fe doped TiO <sub>2</sub>	1, 6, 8, 12 mol.%	RT	Oxygen vacancies, presence of impurities	0.68, 1.3, 0.15, 0.051 μ <sub>B</sub> /Fe.	[42]
Anatase Fe Doped TiO <sub>2</sub>	Fe 4–8 at %	RT	Ti <sup>3+</sup> defect, oxygen vacancies, Fe, BMP	0.5 to 0.7 μ <sub>B</sub> /Fe	[43]
Co doped TiO <sub>2</sub>	3, 5, 7, 10 mol.%	RT	Charge imbalance, lattice distortion and oxygen vacancies	0, 1.0, 1.1, 1.5 μ <sub>B</sub>	[45]
Ga Doped Rutile TiO <sub>2</sub>	6%	350 K	Oxygen vacancies, ionic radii of dopant	18 emu/cm <sup>3</sup>	[46]
TiO <sub>2</sub> on rGO			Healing effect, rGO interaction with Ti <sup>3+</sup> -oxygen vacancies		[47]

#### 4. SnO<sub>2</sub> and Ferromagnetism

SnO<sub>2</sub> has various useful properties alike O-vacancies, pellucidity, excellent charge carrier, high thermal and chemical stability due to which it is used for spin electronic devices [48–50]. SnO<sub>2</sub> nanoparticles have various properties than their bulk oxide, such as the size of SnO<sub>2</sub> is reduced to nanoparticle range, then non-ferromagnetic oxide shows ferromagnetic character [26,51]. Chang et al. investigated that undoped tin oxide shows the ferromagnetic character at room temperature and also explained the importance of O-vacancy in ferromagnetic nature [52]. When the size of various DMS reduced to below 20 nm, then they show excellent ferromagnetic character as compared to when the size is more significant than 100 nm [53].

The magnetic and electronic characteristics of Mo doped with SnO<sub>2</sub> is studied with the help of gradient approximation from density functional theory. Spin functionality is induced on the DOS when the Sn atom is substituted by Mo atom in the crystal structure and this substitution is helpful to make easy the hybridization between the *d*-orbital of Mo and *p*-orbital of O atom. Due to this *p-d* hybridization, in *d*-state of splitting Mo atom spin that is responsible for antisymmetric DOS at the E<sub>F</sub> and this splitting in the high range can generate the magnetism at the site of Mo atom. These samples show excellent spin polarization value at the E<sub>F</sub>. Due to excellent spin polarization value, it can be used in devices that are based on electronic-spin for future respect [54].

The superconducting quantum interference device (SQUID) measurements 5K and 300K for 1% and 2% Fe doped SnO<sub>2</sub> nanoparticles synthesized via chemical co-precipitation method indicate negative effect of doping due to the substitution of dopant ions in the host lattice [55]. Importantly, electron trapped in oxygen vacancies due to Fe<sup>3+</sup>-Vo<sup>2-</sup>-Fe<sup>3+</sup> cluster in the host lattice will compensate with two irons through F centers and leads to surprising FM ordering. Similarly, surfactant-less Co-doped SnO<sub>2</sub> nanocrystals prepared using hydrothermal process showed that introduction of Co (II) ions deforms the SnO<sub>2</sub> lattice resulting in reduction in unit cell volume with Co content without the Co-rich clusters. Linear magnetic response with maximum saturation magnetization (3.5 emu/g) of the flower-like morphology with a Co/SnO<sub>2</sub> mass ratio = 0.06 m/m was found. Ogale et al. predicted that Co-doped SnO<sub>2</sub> films synthesized by pulsed laser deposition technique grown on R plane sapphire show ferromagnetism at high-temperature. The 5% Co-doped film shows a high magnetic moment with a considerable value of 7 ± 5 μB per Co ion and Curie temperature (T<sub>c</sub>) at 650 K [12]. 5% Co-doped SnO<sub>2</sub> was synthesized by Srinivas et al. using the tartaric gel method and investigated RTFM due to oxygen vacancies, vacancy clusters and surface diffusion of Co ions [56]. As the concentration of Co ions increases, the magnetic character also increases in Co-doped SnO<sub>2</sub> and as Mn ions doped with Co ions in SnO<sub>2</sub> lattice, the samples show superparamagnetic character instead of ferromagnetic character (Figure 7) [57].

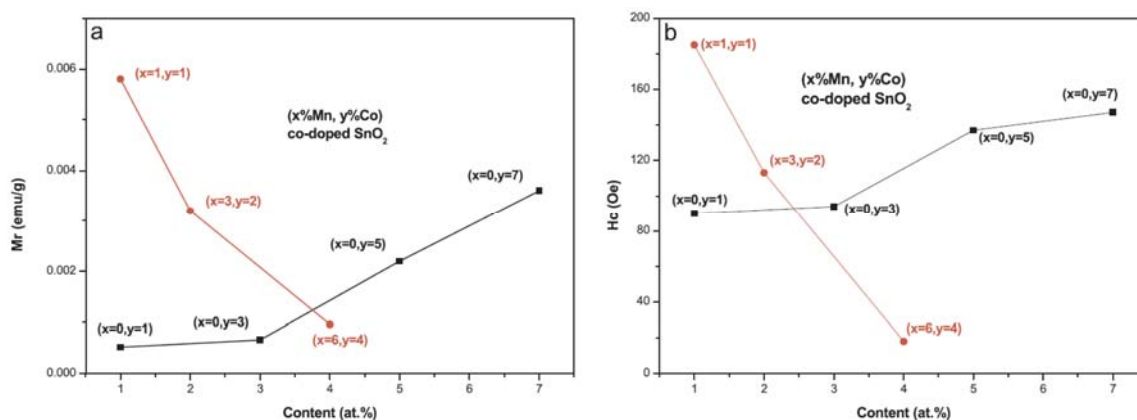


**Figure 7.** (a,b) Magnetization response of  $M_r$  and coercivity field  $H_c$  of the prepared Sn<sub>1-x-y</sub>Mn<sub>x</sub>Co<sub>y</sub>O<sub>2</sub>, respectively (The Figure was reproduced with copyright permission from reference [57]).

The value of lattice constants and the absorption gap are changed as the concentration of Mn ions increases in SnO<sub>2</sub> films and also shows paramagnetic character, which is confirmed by magnetization measurements [58]. When SnO<sub>2</sub> is doped with some 3*d*-transition metals such as Cr, Mn, Fe, Co and Ni ions, then it shows the ferromagnetic character at room temperature and these samples can be synthesized via pulsed-layer deposition method. Among these metal ions, Fe shows the highest magnetic moment and also found that the magnetic moment is independent with the concentration of doping ions [59]. Roy et al. investigated that when SnO<sub>2</sub> is doped with all 3*d*-transition metals one by one, then all 3*d*-transition metals show magnetic character whose moment values are from 0.8 μB to 5.95 μB except Sc, Ti and Ni transition metals (Figure 8). It was found that electronegativity of metal dopants show significant role for ferromagnetic behavior. Among the seven transition metals, Mn shows the highest magnetic moment and Cu shows the lowest magnetic moment value. Remaining all five transition metals shows more stable ferromagnetic states than anti-ferromagnetic states and also observed that Zn doped on SnO<sub>2</sub> have the highest stable ferromagnetic states among all transition metals which can be used as one of the suitable spintronics material [29]. Furthermore, Delgado et al. reported undoped and Zn-doped SnO<sub>2</sub> with flower-like morphology from acicular nanoparticles (NPs) synthesized via hydrothermal method. The morphology of the NPs can be tuned on Zn-doping from truncated rods to sharp needles due to surface free energy of the NPs' facets and growth direction. Higher ferromagnetic ordering was observed in Zn-doped samples due to Zn in Sn lattice positions (ZnSn) as compared with the undoped formulation. Further investigation using thermal annealing under reducing pressure leads to the an excess of V<sub>O</sub>, while, reduced magnetization suggests ZnSn defects controlled magnetism [60].

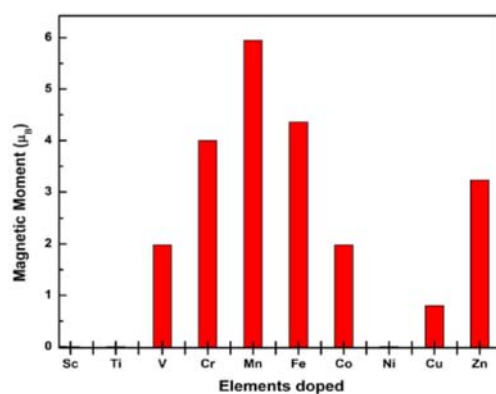


**Figure 8.** Magnetic moment in SnO<sub>2</sub> lattice doped with different transition metal ions (The Figure was reproduced with copyright permission from reference [29]).

Similarly, Co<sup>2+</sup>-doped SnO<sub>2</sub> shows an increase in magnetization with the Co<sup>2+</sup> ions and the average crystallite size estimated to be 10 ± 2 nm for the synthesized nanocrystals. In addition to this, Mn can also influence the magnetization of this composition, i.e., Mn<sup>2+</sup> ions transform the ferromagnetism to superparamagnetism. On the contrary, Sn<sub>0.83</sub>Mn<sub>0.12</sub>Co<sub>0.05</sub>O<sub>2</sub> exhibits diamagnetism with Mn<sup>2+</sup> ions [57]. M-H (magnetic field-magnetization) hysteresis loop demonstrated the room temperature ferromagnetism for the mixed doped (Co, Zn) SnO<sub>2</sub> composition. First-principles calculation estimates the increase of total magnetic moment with effective magnetic interactions between metal ions and oxygen atoms as suggested by experimental methods [61]. The doping of Cr<sup>3+</sup> at Sn<sup>4+</sup> lattice in SnO<sub>6</sub> octahedra enhances the defects, i.e., oxygen vacancies to generate the RTFM via magnetic exchange interaction mediated F centers of oxygen vacancies and magnetic dopant impurities. However, excess Cr of beyond 2%, of solubility limits, decreases the magnetic moment significantly due to antiferromagnetic exchange interaction from interstitial Cr dopants governing over the BMP mechanism [62]. Interestingly, tetragonal shaped nanoparticles (10–40 nm) of Ni doped SnO<sub>2</sub>

showed room-temperature ferromagnetic properties with remarkable  $M_s$  ( $5 \times 10^{-4}$  emu/g) and the coercive field,  $H_c$  83-96 Oe with variable Ni content [63].

$\text{SnO}_2$  doping with Ce exhibits room-temperature ferromagnetic behavior [64] which increases with Ce concentration due to exchange mechanism between  $4f$  and  $5d$  conduction electrons (Figure 9). Notably, divergence between the ZFC and FC measurements concluded that both the Ce ions and  $V_O$  attribute to RT ferromagnetism. Kumar et al. investigated the codoping with rare earth, Er and fluoride ion also induced strong RT ferromagnetism in  $\text{SnO}_2$  as compared to Er doped  $\text{SnO}_2$  [65]. Observed RTFM is due to high oxygen vacancies and shallow defects present in codoping nanoparticles. Conversely, rare-earth doped  $\text{SnO}_2$  including Sm- $\text{SnO}_2$  showing ferromagnetism at RT can also exhibit utilization in magneto-optoelectronic devices [64–66]. Nomura et al. investigated the effects of codoping on  $\text{SnO}_2$  synthesized by the sol-gel route and found that coping enhanced FM as compared to a single dopant [67]. Various dopants (Mn, Co, C, Cr, Mg, V, Fe, Ni, Zn, K) have been studied in detail to use  $\text{SnO}_2$  for RTFM [68–80]. Table 2 briefly summarizes the literature on  $\text{SnO}_2$ .

**Table 2.** Reports on magnetism data on  $\text{SnO}_2$  with various dopants.

Compound	Temperature	Magnetization	% Doping	Reason Of Magnetism	Ref.
$\text{SnO}_2$	300 K			Trapping electrons in oxygen vacancies are polarized, nanosized materials	[26]
Fe doped $\text{SnO}_2$	300 K				[55]
Co doped $\text{SnO}_2$			2–10 mass %	Oxygen vacancies	[81]
Co doped $\text{SnO}_2$	650 K	7 $\mu\text{B}$ per Co ion	5%	Oxygen vacancies	[12]
Co doped $\text{SnO}_2$	RT	0.007–0.09 emu/g	5%	oxygen vacancies, vacancy clusters and surface diffusion of Co ions	[56]
Co and Mn codoped $\text{SnO}_2$	Variable temp		1–12% Mn & 5% Co	Conc. Of Mn ions, defects	[57]
Co and Zn codoped $\text{SnO}_2$					[61]
Cr doped $\text{SnO}_2$	RT		5 mol.%	Oxygen vacancies and magnetic ion impurities	[62]
Ni doped $\text{SnO}_2$	RT	$5 \times 10^{-4}$ emu/g	-	Impurities and structural defects, oxygen vacancies	[63]
Zn doped $\text{SnO}_2$					[60]
Ce doped $\text{SnO}_2$	RT	0.16 to 0.37 emu/g	2, 4, 6 mol.%	Ce in +3 oxidation state, Interaction of bound charge carriers in the defects with Ce ion, oxygen vacancies	[64]
Er, F codoped $\text{SnO}_2$	RT		1 mol.%	Oxygen vacancies, shallower defects	[65]
Er doped $\text{SnO}_2$	RT		1 mol.%	Oxygen vacancies, shallower defects	[65]
Co and Fe codoped $\text{SnO}_2$	RT	-	Co = 0.5–3 mol % Fe = 5 mol %	Interfacial oxygen vacancy defects, exchange interaction between ions, surface of the nanomaterials and electronic factors, Codoping enhance FM, double exchange interaction, oxygen vacancies	[67]
Mn doped $\text{SnO}_2$	Room temp.	~0.98 emu/g	1%		[68]

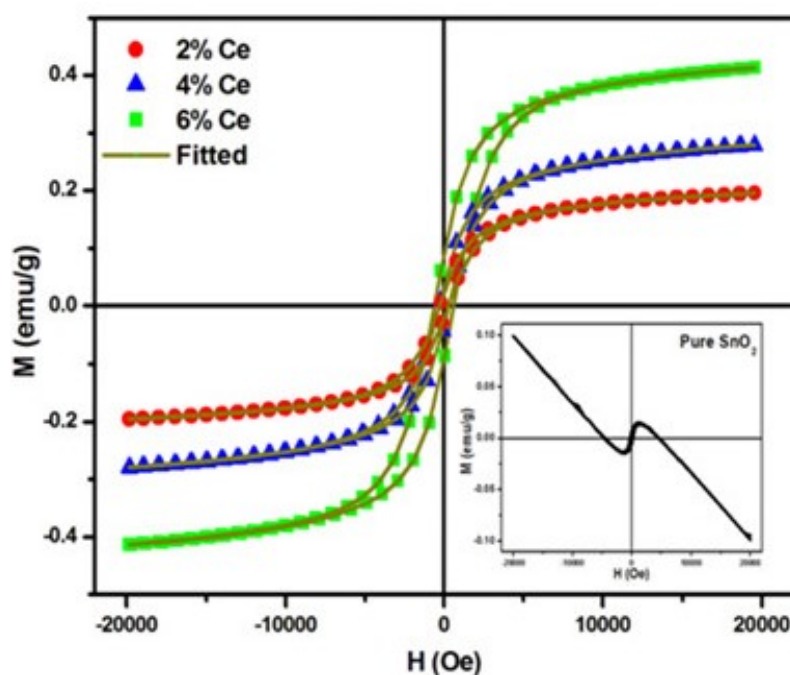


**Figure 9.** M-H hysteresis loop of Ce doped SnO<sub>2</sub> NPs and inset shows M-H curve of undoped SnO<sub>2</sub> NPs (The Figure was reproduced with copyright permission Springer from reference [64]).

## 5. Doping in ZnO and Ferromagnetism

ZnO is *n*-type semiconductor with a wide band of 3.30 eV (exciton binding energy = 60 meV). The benefit of these materials having high stability for high-temperature uses and good photo-response and well-known doping and defect studies makes ZnO smart materials for spintronic application as compared to II-VI compounds [26,82–84]. ZnO exhibits room-temperature ferromagnetism, while the intensity of the ferromagnetism enhanced in the presence of a magnetic field during the synthesis process along with surface morphology changes [84]. Furthermore, FM in ZnO doped with TM ions is primarily due to defect arrangements [85,86]. Additionally, incorporation of Zn<sup>2+</sup> ions in ZnO thin film enhanced RTFM synthesized on Si wafer by RF sputtering method leads to defects in the lattice, causing an alteration in electrical and magnetic properties [87]. This magnetic behavior is usually arbitrated due to defects on insertion of TM ions as dopants and hence, termed as defect-induced *d*<sup>0</sup> FM. While the exact mechanism is still controversial. X-ray centered microscopy and spectroscopy techniques can be helpful to find the intrinsic origin of *d*<sup>0</sup> FM in undoped ZnO, which would be attributed to the O2*p* orbitals arising from zinc vacancies (V<sub>Zn</sub>). *d*<sup>0</sup> FM can be promoted by stabilize V<sub>Zn</sub> in ZnO, appropriate TM ions doping, maintaining crystalline structure [84]. Dietl et al. reported ferromagnetism in metal nitrides and oxides, *p*-type Mn-doped ZnO and GaN semiconductors by theoretical calculations using local spin density approximation [88,89]. In addition, it was experimentally revealed that the Curie temperature (*T*<sub>c</sub>) and exchange interaction are effected by number of holes in the valence band above room temperature.

Sharma et al. have reported the synthesis of hexagonal phase of Er (1, 3, 5, 7%) doped ZnO cone-like nanostructures using the wet chemical route. Ferromagnetic hysteresis loops were observed on Er doped ZnO. Moreover, saturation magnetization (*M*<sub>S</sub>), remanent magnetization (*M*<sub>R</sub>) and the coercivity (*H*<sub>C</sub>) increase with Er concentration (Figure 10) shows DMS properties [90].

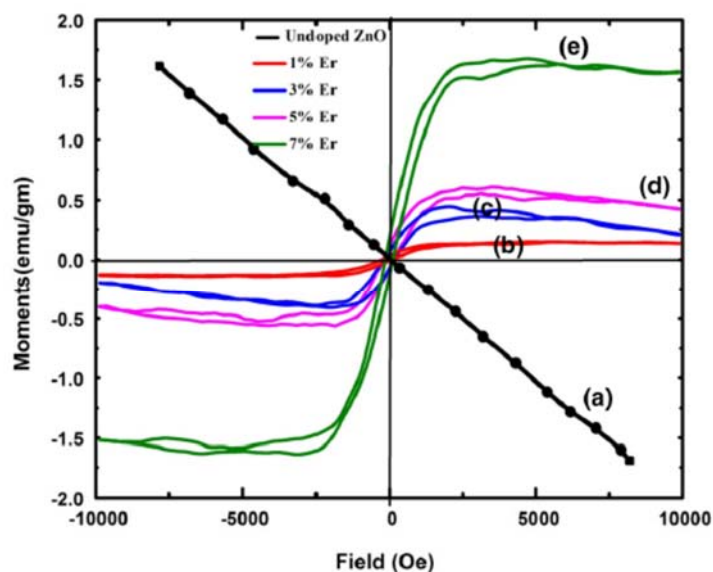


**Figure 10.** M-H curve of (a) pure, (b) 1%, (c) 3%, (d) 5% and (e) 7% Er doped ZnO (The Figure was reproduced with copyright permission Springer from reference [90]).

Hexagonal wurtzite structure has been reported for Fe doped ZnO studied by high-temperature route and shows room temperature magnetization behavior on the addition of Fe ion into ZnO lattice as shown in Figure 11 [91]. Elilarassi et al. synthesized Fe:ZnO by sol-gel combustion method using glycine with wurtzite structure for different Fe concentrations (2, 4, 6 and 8% denoted as F1, F2, F3 and F4). Hysteresis loop promotes ferromagnetic behavior for different Er concentration in ZnO found suitable for spintronics applications (Figure 12) [92]. The FM based on the Ruderman–Kittel Kasuya–Yosida (RKKY) type indirect exchange interaction where  $sp-d$  exchange interaction is between  $Fe^{3+}$  ions and the free carriers of the conduction band of ZnO.

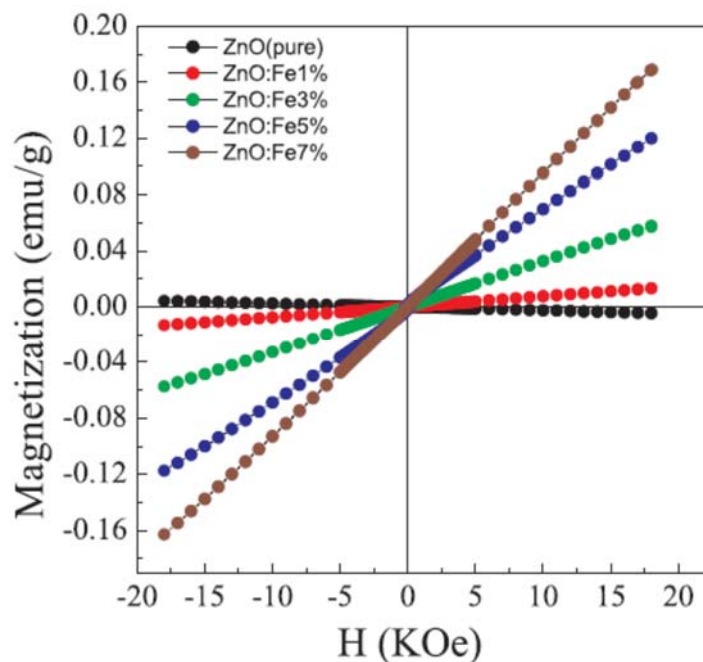


**Figure 11.** M-H hysteresis loops for Fe doped ZnO (The Figure was reproduced with copyright permission from reference [91]).

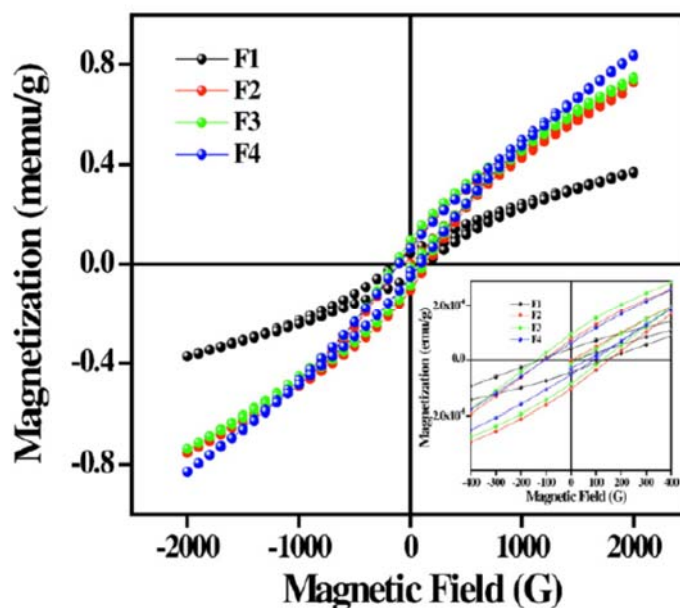


**Figure 12.** M-H curve of Fe doped ZnO (2, 4, 6, 8% F1–F4). Inset shows the M-H curve range –400 to 400 G (The Figure was reproduced with copyright permission from reference [92]).

Fe doped zinc oxide promotes higher  $M_s$  values than undoped due to defects and exchange interaction  $\text{Fe}^{3+}$  ions via BMP mechanism with conductive electrons of ZnO which leads to the spin polarization [92]. The  $M$  vs.  $H$  hysteresis loop at RT shows paramagnetic behavior in the Fe-doped ZnO samples (Figure 10) and the signal increases Fe concentration [26]. Fe (1, 3, 5, 7%) doped ZnO was synthesized by a solid-state high-temperature method. With the increase in the concentration Fe, the inverted spinel  $\text{ZnFe}_2\text{O}_4$  phase was obtained, which results in a gradual rise in the paramagnetic behavior in the ZFO samples [91]. It was observed that magnetization also depends upon synthetic procedure and for obtaining strong FM properties, low-temperature method is more suitable than a solid state synthetic method [66,69]. However, Torquato et al. reported DMO Co-doped ZnO with variable concentration achieved by combustion reaction claimed ferromagnetic behavior above room temperature.  $\text{Co}^{+2}$  doping increases  $M_s$  and also  $T_c$ , which showed that this materials can be beneficial for DMS [93]. Co-doped ZnO thin films were synthesized by dip-coating technique and showed strong ferromagnetism. Various defects, oxygen vacancies and zinc interstices increase with the increase in Co concentration, which supports suitable candidates for room-temperature ferromagnetism [94].

RT ferromagnetism is shown by Mn-doped ZnO nanoparticles films which was synthesized by sol-gel dip coating method at different withdrawal speed [95]. As the withdrawal speed of the coating increases, the bandgap of Mn-doped ZnO decreases from 3.74 eV to 2.76 eV and magnetic behavior increases with the thickness of the thin film. Strong magnetic ordering is disclosed to room temperature (RT) by the Er implanted and annealed ZnO nanoparticles. Due to intrinsic defects, ZnO shows ferromagnetic behavior, which is responsible for the mediator in the magnetic ordering in Er and annealed zinc oxide [96]. The common reason responsible for magnetic response in the oxides is due to the existence of oxygen vacancy. For the continuation of steady magnetic behavior, extensive effort and inclusion of dopants must be demanding conditions in these oxides [97]. Due to doping of Mn is doped in ZnO, the shape and extent of the electron spin resonance (ESR) spectra are changed. From these changes, it shows that a dilute magnetic semiconductor character is fabricated in ZnO. It has been reported that the concentration of doped Mn is 0.6%, then it shows a sharp resonance peak and if the concentration of doped Mn is greater than 0.8%, then there is a decrease in the intensity (Figure 13) [98]. Hence, the appropriate level of dopants in metal oxide lattice help to find DMSOs.

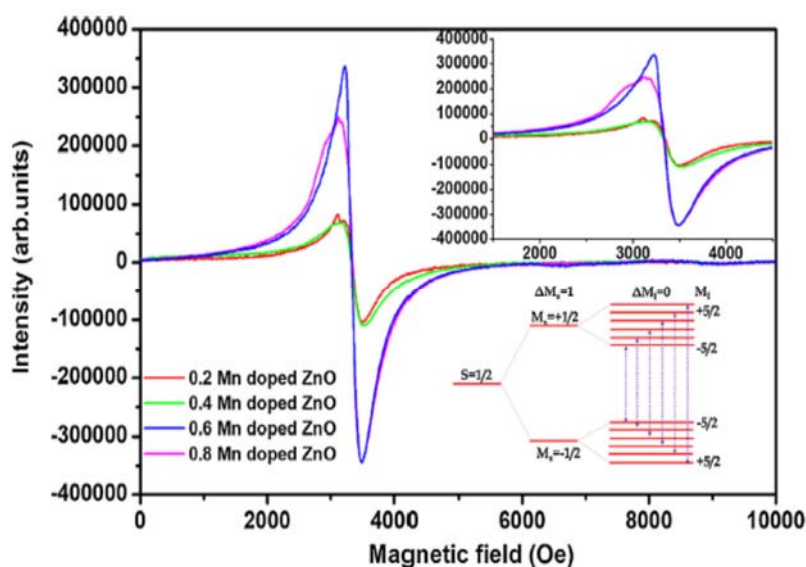


**Figure 13.** ESR spectra of Mn-doped ZnO as a function of Mn contents (The Figure was reproduced with copyright permission from reference [98]).

Zinc oxide films and copper-doped zinc oxide films was casted using screen-printing techniques a eco-friendly. As copper is doped on zinc oxide films, it increases the O-vacancies, which was confirmed by EPR signal obtained at  $g$  value 2.0018 [99]. Hence, these materials may be used in spin electronics and electro-optics devices. Table 3 provides a brief summary of the literature on ZnO.

**Table 3.** Reports on magnetism data on ZnO with various dopants.

Compound	Temperature	% Doping	Reason for FM	Ref.
ZnO	300 K	-	Exchange interactions between localized electron spin moment with oxygen vacancies, defects, nanomaterials	[26,84]
Zn doped ZnO	300 K	-	Defects, $Zn_i$ , annealing in presence of magnetic field from north to south, BMP model	[87]
Er doped ZnO	RT	1, 3, 5, 7 at %	Oxygen vacancies, defects	[90]
Fe doped ZnO	RT	1, 3, 5, 7%	grain boundary barrier defect, interstitial Zn defect, oxygen vacancies	[91]
Co doped ZnO	RT	2, 3, 7, 10 mol.%	Oxygen vacancies, defects	[93]
Co-doped ZnO	RT	1, 3, 5 mol.%	Oxygen vacancies, Zn interstices	[94]
Fe doped ZnO	RT	2, 4, 6, 8%	RKKY exchange interaction, oxygen vacancies, defects	[92]
Mn-doped ZnO	RT	Variable thickness of films	Higher the thickness of the film, oxygen vacancies	[95]
Mn doped ZnO	RT	0.2, 0.4, 0.6, 0.8 Mn/ZnO weight ratio	Synergic effect caused by oxygen vacancies and defects	[98]
Cu doped ZnO		4 mol.%	Oxygen vacancies	[99]

## 6. Doping in $In_2O_3$ and Ferromagnetism

Several reports demonstrating ferromagnetism at RT for TM-ion doped- $In_2O_3$  bulk/thin film were available in the literature [3,100,101]. In this way, ferromagnetism shown by Laser ablated transition-metal (TM)-doped  $In_2O_3$  thin films grafted on  $MgO$  and  $Al_2O_3$  substrates [102], milled  $In_2O_3$  powder [103], to name a few.

The RF-sputtered film of Fe, Cu codoped  $\text{In}_2\text{O}_3$  shows interesting local structural, optical, magnetic and transport properties [104]. Importantly, interexchange mechanism and overlapping of polarons via BMP explained the observed ferromagnetism. However, changing the synthesis protocol such as spin coating techniques and concentration of Fe highly affect the magnetic properties (Figure 14) [105]. As the concentration of Fe increases FM decreases due to disappearance of nearest neighbor hopping (NNH) conduction, whereas sol gel method used for Fe doped  $\text{In}_2\text{O}_3$  followed by annealing at 300–600 °C in presence of  $\text{H}_2$  showed similar magnetization behavior [106]. Strong interaction of localized electrons with Fe ions to polarize its spin cause magnetic behavior and ferromagnetism decreases as oxygen vacancies decreases on increasing Fe concentration.

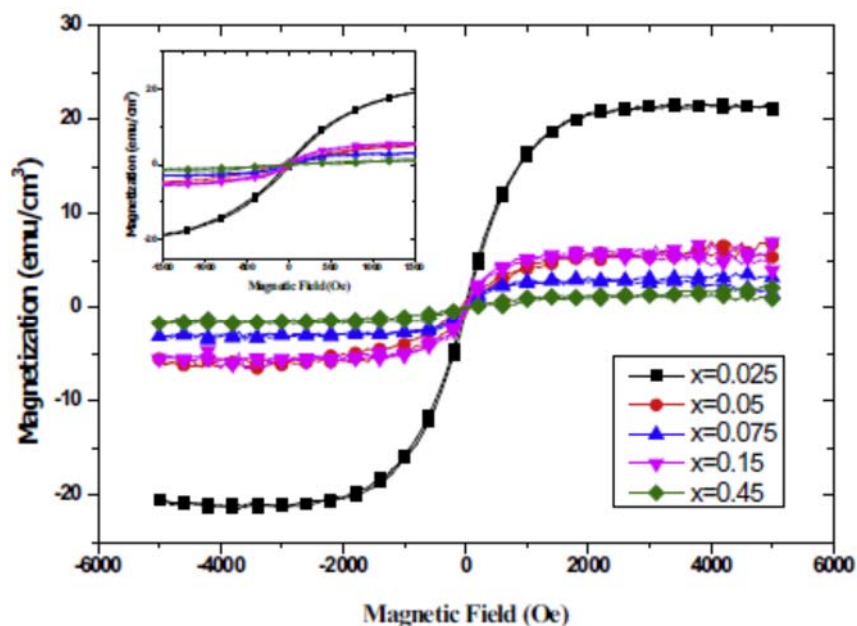


**Figure 14.** M vs. H hysteresis loop for  $\text{In}_2\text{O}_3$  films with different composition of Fe ( $x = 0.025$ – $0.45$ ). Inset shows the magnified view of low field curve (The Figure is reproduced with copyright permission [105]).

Some other methods, such as 5% Fe-doped  $\text{In}_2\text{O}_3$  films which were pulsed laser deposited under a partial pressure of  $10^{-3}$ ,  $10^{-5}$  and  $10^{-7}$  torr, respectively [107] and polarized neutron scattering measurements reveal lower magnetized Fe-rich phase located at the interface than uniformly distributed phases. A similar study was reported by Garnet et al. showing ferromagnetic ordering with decreased saturation magnetization with concentration for Fe in  $\text{In}_2\text{O}_3$  nanocrystalline films prepared by the sol-gel method [108]. Similarly, Fe doped  $\text{In}_2\text{O}_3$  synthesized by solid-state reaction method and vacuum annealing with various levels of dopants [109]. Mn-doped  $\text{In}_2\text{O}_3$  was synthesized by solid-state methods and that composition showed magnetic moment of  $2.83 \mu\text{B}/\text{Mn}$  due to tetrahedrally or octahedrally coordinated  $\text{Mn}^{3+}$  in the intermediate spin state [110]. A mesoporous  $\text{In}_2\text{O}_3$  semiconductor implanted with Co ions shows a measurable ferromagnetic signature at RT [111]. Co-doped  $\text{In}_2\text{O}_3$  synthesized by chemical solution route showed FM at RT and LT [112]. It is observed that the Bohr magneton number remained consistent at a lower doping concentration of  $\text{Co}^{2+}$  in the high spin state while it decreased on the addition of  $\text{Co}^{3+}$  ions. On the contrary, Figure 15 shows the N-doped  $\text{In}_2\text{O}_3$  films, which exhibited room-temperature (RT) ferromagnetism and Mott variable range hopping (VRH) transport behavior [113]. Moreover, alkali metal-based doping such as Li-doped  $\text{In}_2\text{O}_3$  nanoparticles exhibits  $d^0$  ferromagnetism at room temperature via FM coupling exerted by the  $\text{LiIn-ONN-VIn-ONN-LiIn}$  chains [114]. Table 4 provides a short summary on recent reports on  $\text{In}_2\text{O}_3$ .

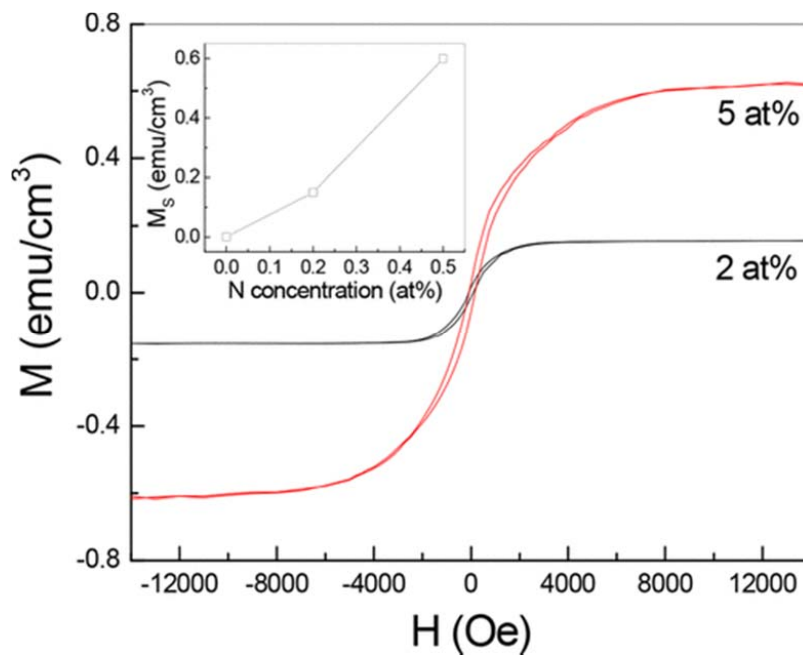


**Figure 15.** Magnetic hysteresis loops of N-doped  $\text{In}_2\text{O}_3$  films with 2 and 5 at.% ratio of N recorded at 300 K (Reprinted with permission from American Chemical Society [113]).

**Table 4.** Reports on magnetism data on  $\text{In}_2\text{O}_3$  with various dopants.

Materials	Dopants %	Temp.	Reason for Magnetism	Value of Magnetism	Ref.
Pure $\text{In}_2\text{O}_3$	-	RT	Defect induced in $\text{In}_2\text{O}_3$ formed by mechanical mining, oxygen deficient surfaces		[3,100,101]
Fe, Cu codoped $\text{In}_2\text{O}_3$	$0.06 \leq x \leq 0.20$	RT	s-pd interexchange mechanism and overlapping of polarons	2.52 $\text{emu}/\text{cm}^3$ to 7.2 $\text{emu}/\text{cm}^3$ when x goes from 0.06 to 0.20	[104]
Fe doped $\text{In}_2\text{O}_3$	2.5%		Defect like oxygen vacancy or surface passivation defects that could be created by hydrogen- annealing, mixed valence of Fe	2–30 $\text{emu}/\text{cm}^3$	[106]
Fe doped $\text{In}_2\text{O}_3$	2.5–45%		Oxygen vacancies and it decreases on increasing Fe concentration, BMP		[105]
Fe doped $\text{In}_2\text{O}_3$	5%	LT	BMP, magnetization increases on decreasing partial pressure of $\text{O}_2$ ,		[107]
Fe doped $\text{In}_2\text{O}_3$	1.8, 2.5%	RT	Interfacial and local defects		[108]
Fe doped $\text{In}_2\text{O}_3$	3, 5, 7%	RT	Magnetic ions and defects formed during annealing	11.56 $\text{memu}/\text{g}$ to 148.64 $\text{memu}/\text{g}$	[109]
Mn doped $\text{In}_2\text{O}_3$	10%	LT	Tetrahedrally or octahedrally coordinated $\text{Mn}^{3+}$ in the intermediate spin state	2.83 $\mu\text{B}/\text{Mn}$	[110]
Co doped $\text{In}_2\text{O}_3$	<0.044 and >0.052	LT and RT	Ferromagnetism at RT observed only annealing in high vacuum due to oxygen vacancies, magnetic susceptibility of all the specimens decreases with an increase in the temperature		[112]
Co doped $\text{In}_2\text{O}_3$			Oxygen vacancies		[111]
N doped $\text{In}_2\text{O}_3$		RT	N-induced acceptor defects, oxygen vacancies,		[113]
Li doped at.% $\text{In}_2\text{O}_3$	(0.5 to 7)		Indium vacancies on substituting by Li ions	1.64 to 4.06 $\mu\text{B}$	[114]

## 7. Conclusions

To summarize, the review article has attempted to provide the insights regarding the structural analysis, magnetic properties of DMSO with various ferromagnetic or paramagnetic dopants into binary metal oxide nanomaterials which exhibit a ferromagnetic behavior at or above room temperature. Several factors govern the DMS in which oxygen vacancies, interstitial defects, particle size, especially in the nano range, synthesis methods are the probable reasons. It is believed the ferromagnetism arises due to the exchange interactions between unpaired electron spins emerging from oxygen vacancies at the surfaces of the nanomaterials. The oxygen vacancies present at the surface and subsurface, the presence of deeper, shallower and grain boundary barrier defects, interstitial metal defects, charge imbalance, formation of metallic clusters, electronic defects are responsible for FM even annealing temperature, with or without vacuum largely affecting it. Further, exchange interaction between localized electron spin moment with oxygen vacancy and annealing the NMs in the presence of magnetic field from North to South pole also enhances the FM. Moreover, size of the nanomaterials reduced to below 20 nm, excellent FM was achieved at or above room temperature. The probable mechanism of DMS is still debatable and controversial field among the various researchers. Most of the host materials as the dopant concentration increase at concentration level below 10%, it found suitable for DMS. The origin of DMSO could be explained on the basis of the BMP theory. However, still more work has to be done for clear understanding and governing of defects-induced ferromagnetism in non-magnetic bulk materials. Importantly, these materials can be easily integrated in spin-devices for long life-time of spin-alignment and additionally, it is proposed that can also overcome the spin-scattering at the interfaces to avoid data loss. Of course, these nanomaterials are a potential materials for spintronics device due high spin polarization and high  $T_c$  without the doping of expensive inner-transition metal in general. There is much promising in this field as it may open a novel gateway for feasible efficient spintronics at room temperature in nanometric regime.

**Author Contributions:** A.G. and R.Z. did extensive research on literature. P.K. worked on conceptualization and validation. V.K. and A.K. worked on review and overall editing of manuscript. All authors have read and agreed to the published version of the manuscript.

**Funding:** This research received no external funding.

**Conflicts of Interest:** The authors declare no conflict of interest.

## References

1. Dietl, T. A ten-year perspective on dilute magnetic semiconductors and oxides. *Nat. Mater.* **2010**, *9*, 965. [[CrossRef](#)]
2. Ning, S.; Zhan, P.; Xie, Q.; Wang, W.; Zhang, Z. Defects-Driven Ferromagnetism in Undoped Dilute Magnetic Oxides: A Review. *J. Mater. Sci. Technol.* **2015**, *31*, 969–978. [[CrossRef](#)]
3. Lemine, O.; Bououdina, M.; Alyamani, A.; Omri, K.; Ibnaouf, K.; Ibrahim, M.A.; Alhathloul, R. Defect-induced room temperature ferromagnetism in mechanically milled nanocrystalline  $\text{In}_2\text{O}_3$  powder. *Mater. Lett.* **2016**, *181*, 152–155. [[CrossRef](#)]
4. Coey, J.M.D.; Chambers, S.A. Oxide Dilute Magnetic Semiconductors—Fact or Fiction? *MRS Bull.* **2011**, *33*, 1053–1058. [[CrossRef](#)]
5. Coey, J.M.D. Dilute magnetic oxides. *Curr. Opin. Solid State Mater. Sci.* **2006**, *10*, 83–92. [[CrossRef](#)]
6. Coey, J.M.D.; Venkatesan, M.; Fitzgerald, C.B. Donor impurity band exchange in dilute ferromagnetic oxides. *Nat. Mater.* **2005**, *4*, 173–179. [[CrossRef](#)]
7. Matsumoto, Y.; Murakami, M.; Shono, T.; Hasegawa, T.; Fukumura, T.; Kawasaki, M.; Ahmet, P.; Chikyow, T.; Koshihara, S.; Koinuma, H. Room-temperature ferromagnetism in transparent transition metal-doped titanium dioxide. *Science* **2001**, *291*, 854–856. [[CrossRef](#)]
8. Yamada, Y.; Ueno, K.; Fukumura, T.; Yuan, H.T.; Shimotani, H.; Iwasa, Y.; Gu, L.; Tsukimoto, S.; Ikuhara, Y.; Kawasaki, M. Electrically induced ferromagnetism at room temperature in cobalt-doped titanium dioxide. *Science* **2011**, *332*, 1065–1067. [[CrossRef](#)]

9. Saadaoui, H.; Luo, X.; Salman, Z.; Cui, X.Y.; Bao, N.N.; Bao, P.; Zheng, R.K.; Tseng, L.T.; Du, Y.H.; Prokscha, T. Intrinsic ferromagnetism in the diluted magnetic semiconductor Co: TiO<sub>2</sub>. *Phys. Rev. Lett.* **2016**, *117*, 227202. [CrossRef]
10. Wang, D.; Chen, Q.; Xing, G.; Yi, J.; Rahman, B.S.; Ding, J.; Wang, J.; Wu, T. Robust room-temperature ferromagnetism with giant anisotropy in Nd-doped ZnO nanowire arrays. *Nano Lett.* **2012**, *12*, 3994–4000. [CrossRef]
11. Lee, J.J.; Xing, G.Z.; Yi, J.B.; Chen, T.; Ionescu, M.; Li, S. Tailoring the coercivity in ferromagnetic ZnO thin films by 3 d and 4 f elements codoping. *Appl. Phys. Lett.* **2014**, *104*, 012405. [CrossRef]
12. Ogale, S.; Choudhary, R.J.; Buban, J.P.; Lofland, S.E.; Shinde, S.R.; Kale, S.N.; Kulkarni, V.N.; Higgins, J.; Lanci, C.; Simpson, J.R. High Temperature Ferromagnetism with a Giant Magnetic Moment in Transparent Co-doped SnO<sub>2-δ</sub>. *Phys. Rev. Lett.* **2003**, *91*, 077205. [CrossRef]
13. Nagarajan, R.; Kumar, V.; Ahmad, S. Anion Doped Binary Oxides, SnO<sub>2</sub>, TiO<sub>2</sub> and ZnO: Fabrication Procedures, Fascinating Properties and Future Prospects. *Indin J. Chem. A* **2012**, *51A*, 145–154.
14. Madian, M.; Eychmüller, A.; Giebeler, L. Current advances in TiO<sub>2</sub>-based nanostructure electrodes for high performance lithium ion batteries. *Batteries* **2018**, *4*, 7. [CrossRef]
15. Dixon, D. Difference in Electrochemical Mechanism of SnO<sub>2</sub> Conversion in Lithium-Ion and Sodium-Ion Batteries: Combined in Operando and Ex Situ XAS Investigations. *ACS Omega* **2019**, *4*, 9731–9738. [CrossRef]
16. López, C.M.; Choi, K.-S. Enhancement of electrochemical and photoelectrochemical properties of fibrous Zn and ZnO electrodes. *Chem. Commun.* **2005**, 3328–3330. [CrossRef]
17. Ogale, S.B.; Venkatesan, T.V.; Blamire, M.G. Introduction to Magnetic Oxides. In *Functional Metal Oxides: New Science and Novel Applications*; John Wiley and Sons, Wiley-VCH Verlag GmbH & Co. KGaA: Hoboken, NJ, USA, 2013; pp. 1–49.
18. Si, S.; Li, C.; Wang, X.; Yu, D.; Peng, Q.; Li, Y. Magnetic Monodisperse Fe<sub>3</sub>O<sub>4</sub> Nanoparticles. *Cryst. Growth Des.* **2005**, *5*, 391–393. [CrossRef]
19. Yang, T.; Shen, C.; Li, Z.; Zhang, H.; Xiao, C.; Chen, S.; Xu, Z.; Shi, D.; Li, J.; Gao, H. Highly Ordered Self-Assembly with Large Area of Fe<sub>3</sub>O<sub>4</sub> Nanoparticles and the Magnetic Properties. *J. Phys. Chem. B* **2005**, *109*, 23233–23236. [CrossRef]
20. Ghazanfari, M.R.; Kashefi, M.; Shams, S.F.; Jaafari, M.R. Perspective of Fe<sub>3</sub>O<sub>4</sub> nanoparticles role in biomedical applications. *Biochem. Res. Int.* **2016**, 2016. [CrossRef]
21. Buschow, K.H.J.; Boer, F.R. *Physics of Magnetism and Magnetic Materials*; Springer: Boston, MA, USA, 2003; Volume 7. [CrossRef]
22. Bedanta, S. Supermagnetism in Magnetic Nanoparticle Systems. *Ph.D. Thesis*. 2007. Available online: <https://nbn-resolving.org/urn:nbn:de:hbz:464-20070226-114713-8> (accessed on 15 March 2020).
23. Frenkel, J.; Doefman, J. Spontaneous and induced magnetisation in ferromagnetic bodies. *Nature* **1930**, *126*, 274–275. [CrossRef]
24. Teja, A.S.; Koh, P.-Y. Synthesis, properties, and applications of magnetic iron oxide nanoparticles. *Prog. Cryst. Growth Charact. Mater.* **2009**, *55*, 22–45. [CrossRef]
25. Hong, N.H.; Sakai, J.; Poirot, N.; Brizé, V. Room-temperature ferromagnetism observed in undoped semiconducting and insulating oxide thin films. *Phys. Rev. B* **2006**, *73*, 132404. [CrossRef]
26. Sundaresan, A.; Bhargavi, R.; Rangarajan, N.; Siddesh, U.; Rao, C.N.R. Ferromagnetism as a universal feature of nanoparticles of the otherwise nonmagnetic oxides. *Phys. Rev. B* **2006**, *74*, 161306. [CrossRef]
27. Ohtsuki, T.; Chainani, A.; Eguchi, R.; Matsunami, M.; Takata, Y.; Taguchi, M.; Nishino, Y.; Tamasaku, K.; Yabashi, M.; Ishikawa, T. Role of Ti 3 d Carriers in Mediating the Ferromagnetism of Co: TiO<sub>2</sub> Anatase Thin Films. *Phys. Rev. Lett.* **2011**, *106*, 047602. [CrossRef]
28. Wang, H.; Cao, X.; Takagiwa, Y.; Snyder, G.J. Higher mobility in bulk semiconductors by separating the dopants from the charge-conducting band—A case study of thermoelectric PbSe. *Mater. Horiz.* **2015**, *2*, 323–329. [CrossRef]
29. Roy, S.; Luitel, H.; Sanyal, D. Magnetic properties of transition metal doped SnO<sub>2</sub>: A detailed theoretical study. *Comput. Condens. Matter* **2019**, *21*, e00393. [CrossRef]
30. Norton, D.P.; Heo, Y.W.; Ivill, M.P.; Ip, K.; Pearton, S.J.; Chisholm, M.F.; Steiner, T. 8 ZnO: Growth, doping & processing. *Mater. Today* **2004**, *7*, 34–40.
31. Ogale, S.B. Dilute Doping, Defects, and Ferromagnetism in Metal Oxide Systems. *Adv. Mater.* **2010**, *22*, 3125–3155. [CrossRef]

32. Hameed, A.S.H.; Karthikeyan, C.; Sasikumar, S.; Kumar, V.N.; Kumaresan, S.; Ravi, G. Impact of alkaline metal ions  $Mg^{2+}$ ,  $Ca^{2+}$ ,  $Sr^{2+}$  and  $Ba^{2+}$  on the structural, optical, thermal and antibacterial properties of ZnO nanoparticles prepared by the co-precipitation method. *J. Mater. Chem. B* **2013**, *1*, 5950–5962. [[CrossRef](#)]
33. Andronenko, S.I.; Misra, S.K. A Review of EPR Studies on Magnetization of Nanoparticles of Dilute Magnetic Semiconductors Doped by Transition-Metal Ions. *Appl. Magn. Reson.* **2015**, *46*, 693–707. [[CrossRef](#)]
34. Choudhury, B.; Paul, S.; Ameen Ahmed, G.; Choudhury, A. Adverse effect of Mn doping on the magnetic ordering in Mn doped TiO<sub>2</sub> nanoparticles. *Mater. Res. Express* **2015**, *2*, 096104. [[CrossRef](#)]
35. Sharma, S.; Chaudhary, S.; Kashyap, S.C.; Sharma, S.K. Room temperature ferromagnetism in Mn doped TiO<sub>2</sub> thin films: Electronic structure and Raman investigations. *J. Appl. Phys.* **2011**, *109*, 083905. [[CrossRef](#)]
36. Akshay, V.R.; Arun, B.; Mandal, G.; Vasundhara, M. Structural, optical and magnetic behavior of sol-gel derived Ni-doped dilute magnetic semiconductor TiO<sub>2</sub> nanocrystals for advanced functional applications. *Phys. Chem. Chem. Phys.* **2019**, *21*, 2519–2532. [[CrossRef](#)] [[PubMed](#)]
37. Hou, D.; Meng, H.J.; Jia, L.Y.; Ye, X.J.; Zhou, H.J.; Li, X.L. Oxygen vacancy enhanced the room temperature ferromagnetism in Ni-doped TiO<sub>2</sub> thin films. *Phys. Lett. A* **2007**, *364*, 318–322. [[CrossRef](#)]
38. Rodriguez-Torres, C.; Cabrera, A.F.; Errico, L.A.; Adán, C.; Requejo, F.G.; Weissmann, M.; Stewart, S.J. Local structure and magnetic behaviour of Fe-doped TiO<sub>2</sub> anatase nanoparticles: Experiments and calculations. *J. Phys. Condens. Matter* **2008**, *20*, 135210. [[CrossRef](#)]
39. Chen, J.; Rulis, P.; Ouyang, L.; Satpathy, S.; Ching, W.Y. Vacancy-enhanced ferromagnetism in Fe-doped rutile TiO<sub>2</sub>. *Phys. Rev. B* **2006**, *74*, 235207. [[CrossRef](#)]
40. Santara, B.; Giri, P.; Dhara, S.; Imakita, K.; Fujii, M. Oxygen vacancy-mediated enhanced ferromagnetism in undoped and Fe-doped TiO<sub>2</sub> nanoribbons. *J. Phys. D: Appl. Phys.* **2014**, *47*, 235304. [[CrossRef](#)]
41. Fajariah, N.; Prabowo, W.A.E.; Fathurrahman, F.; Melati, A.; Dipojono, H.K. The investigation of electronic structure of transition metal doped TiO<sub>2</sub> for diluted magnetic semiconductor applications: A first principle study. *Procedia Eng.* **2017**, *170*, 141–147. [[CrossRef](#)]
42. Mallia, G.; Harrison, N. Magnetic moment and coupling mechanism of iron-doped rutile TiO<sub>2</sub> from first principles. *Phys. Rev. B* **2007**, *75*, 165201. [[CrossRef](#)]
43. Bapna, K.; Phase, D.; Choudhary, R. Study of valence band structure of Fe doped anatase TiO<sub>2</sub> thin films. *J. Appl. Phys.* **2011**, *110*, 043910. [[CrossRef](#)]
44. Ogale, S.; Kundaliya, D.; Mehraeen, S.; Fu, L.-f.; Zhang, S.; Lussier, A.; Dvorak, J.; Browning, N.; Idzerda, Y.; Venkatesan, T. Chemical Inhomogeneity and Mixed-State Ferromagnetism in Diluted Magnetic Semiconductor Co:TiO<sub>2</sub>. *Chem. Mater.* **2008**, *20*, 1344–1352. [[CrossRef](#)]
45. Fukumura, T.; Toyosaki, H.; Ueno, K.; Nakano, M.; Kawasaki, M. Role of charge carriers for ferromagnetism in cobalt-doped rutile TiO<sub>2</sub>. *New Journal of physics* **2008**, *10*, 055018. [[CrossRef](#)]
46. Song, Y.; Wang, X.; Tao, L.; Song, B.; Zhang, L.; Zhang, Y.; Sui, Y.; Liu, Z.; Tang, J.; Han, X. Effect of Ga-doping and oxygen vacancies on the ferromagnetism of TiO<sub>2</sub> thin films. *J. Alloy. Compd.* **2017**, *694*, 929–934. [[CrossRef](#)]
47. Zhu, Q.; Wang, X.; Jiang, J.; Xu, A.-W. Healing effect of graphene oxide in achieving robust dilute ferromagnetism in oxygen-deficient titanium dioxide. *J. Phys. Chem. C* **2017**, *121*, 22806–22814. [[CrossRef](#)]
48. Gordon, R.G. Criteria for choosing transparent conductors. *MRS Bull.* **2000**, *25*, 52–57. [[CrossRef](#)]
49. Wang, N.; Zhou, W.; Liang, Y.; Cui, W.; Wu, P. Oxygen vacancy-mediated room temperature ferromagnetism in Sr-doped SnO<sub>2</sub> nanoparticles. *J. Mater. Sci. Mater. Electron.* **2015**, *26*, 7751–7756. [[CrossRef](#)]
50. Kumar, V.; Govind, A.; Nagarajan, R. Optical and photocatalytic properties of heavily F—doped SnO<sub>2</sub> nanocrystals by a novel single-source precursor approach. *Inorg. Chem.* **2011**, *50*, 5637–5645. [[CrossRef](#)]
51. Sundaresan, A.; Rao, C. Ferromagnetism as a universal feature of inorganic nanoparticles. *Nano Today* **2009**, *4*, 96–106. [[CrossRef](#)]
52. Chang, G.; Forrest, J.; Kurmaev, E.; Morozovska, A.; Glinchuk, M.; McLeod, J.; Moewes, A.; Surkova, T.; Hong, N.H. Oxygen-vacancy-induced ferromagnetism in undoped SnO<sub>2</sub> thin films. *Phys. Rev. B* **2012**, *85*, 165319. [[CrossRef](#)]
53. Maensiri, S.; Sreesongmuang, J.; Thomas, C.; Klinkaewnarong, J. Magnetic behavior of nanocrystalline powders of Co-doped ZnO diluted magnetic semiconductors synthesized by polymerizable precursor method. *J. Magn. Magn. Mater.* **2006**, *301*, 422–432. [[CrossRef](#)]

54. Rai, D.P.; Laref, A.; Shankar, A.; Sandeep; Sakhya, A.P.; Khenata, R.; Thapa, R.K. Spin-induced transition metal (TM) doped SnO<sub>2</sub> a dilute magnetic semiconductor (DMS): A first principles study. *J. Phys. Chem. Solids* **2018**, *120*, 104–108. [[CrossRef](#)]
55. Sharma, M.; Doila, S.N.; Kumar, S.; Alvi, P.A. Effect of Fe Doping on Magnetic Behavior of SnO<sub>2</sub> Nanoparticles for Spintronics Applications. *IOP Conf. Ser. Mater. Sci. Eng.* **2019**, *594*, 012004. [[CrossRef](#)]
56. Srinivas, K.; Vithal, M.; Sreedhar, B.; Raja, M.M.; Reddy, P.V. Structural, optical, and magnetic properties of nanocrystalline Co doped SnO<sub>2</sub> based diluted magnetic semiconductors. *J. Phys. Chem. C* **2009**, *113*, 3543–3552. [[CrossRef](#)]
57. Zhu, S.; Chen, C.; Li, Z. Magnetic enhancement and magnetic signal tunability of (Mn, Co) co-doped SnO<sub>2</sub> dilute magnetic semiconductor nanoparticles. *J. Magn. Magn. Mater.* **2019**, *471*, 370–380. [[CrossRef](#)]
58. Kimura, H.; Fukumura, T.; Kawasaki, M.; Inaba, K.; Hasegawa, T.; Koinuma, H. Rutile-type oxide-diluted magnetic semiconductor: Mn-doped SnO<sub>2</sub>. *Appl. Phys. Lett.* **2002**, *80*, 94–96. [[CrossRef](#)]
59. Fitzgerald, C.; Venkatesan, M.; Dorneles, L.S.; Gunning, R.; Stamenov, P.; Coey, J.M.D.; Stampe, P.; Kennedy, R.; Moreira, E.C.; Sias, U.S. Magnetism in dilute magnetic oxide thin films based on Sn O<sub>2</sub>. *Phys. Rev. B* **2006**, *74*, 115307. [[CrossRef](#)]
60. Paraguay-Delgado, F.; Vasquez, F.C.; Holguín-Momaca, J.T.; Santillán-Rodríguez, C.R.; Matutes-Aquino, J.A.; Olive-Méndez, S.F. Room-temperature ferromagnetism and morphology evolution of SnO<sub>2</sub> flower-like microparticles by Zn-doping. *J. Magn. Magn. Mater.* **2019**, *476*, 183–187. [[CrossRef](#)]
61. Boukhvalov, D.W.; Manikandan, D.; Zhidkov, I.S.; Kukhareenko, A.I.; Cholakh, S.O.; Kurmaev, E.Z.; Murugan, R. Effect of doping and annealing on the electronic structure and magnetic properties of nanoscale Co and Zn co-doped SnO<sub>2</sub>: An experimental study and first-principles modeling. *J. Alloy. Compd.* **2019**, *799*, 433–441. [[CrossRef](#)]
62. URS, K.; Bhat, S.; Kamble, V. On exceeding the solubility limit of Cr+ 3 dopants in SnO<sub>2</sub> nanoparticles based dilute magnetic semiconductors. *J. Appl. Phys.* **2018**, *123*, 161518. [[CrossRef](#)]
63. Pascariu, P.; Airinei, A.; Grigoras, M.; Fifere, N.; Sacarescu, L.; Lupu, N.; Stoleriu, L. Structural, optical and magnetic properties of Ni doped SnO<sub>2</sub> nanoparticles. *J. Alloy. Compd.* **2016**, *668*, 65–72.
64. Ahmed, A.; Siddique, M.N.; Ali, T.; Tripathi, P. Defect assisted improved room temperature ferromagnetism in Ce doped SnO<sub>2</sub> nanoparticles. *Appl. Surf. Sci.* **2019**, *483*, 463–471. [[CrossRef](#)]
65. Kumar, V.; Uma, S.; Nagarajan, R. Optical and magnetic properties of (Er, F) co-doped SnO<sub>2</sub> nanocrystals. *Turk. J. Phys.* **2014**, *38*, 450–462. [[CrossRef](#)]
66. Cao, E.; Zhangf, Y.; Hao, W.; Peng, H.; Sun, L.; Hu, J. Room temperature ferromagnetism in Sm-doped SnO<sub>2</sub> PLD film. *Appl. Surf. Sci.* **2013**, *282*, 376–383. [[CrossRef](#)]
67. Nomura, K.; Okabayashi, J.; Okamura, K.; Yamada, Y. Magnetic properties of Fe and Co codoped SnO<sub>2</sub> prepared by sol-gel method. *J. Appl. Phys.* **2011**, *110*, 083901. [[CrossRef](#)]
68. Ahmed, S. Room-temperature ferromagnetism in pure and Mn doped SnO<sub>2</sub> powders. *Solid State Commun.* **2010**, *150*, 2190–2193. [[CrossRef](#)]
69. Afroj, S.; Karim, N.; Wang, Z.; Tan, S.; He, P.; Holwill, M.; Ghazaryan, D.; Fernando, A.; Novoselov, K.S. Engineering graphene flakes for wearable textile sensors via highly scalable and ultrafast yarn dyeing technique. *ACS Nano* **2019**, *13*, 3847–3857. [[CrossRef](#)]
70. Sabergharesou, T.; Wang, T.; Ju, L.; Radovanovic, P.V. Electronic structure and magnetic properties of sub-3 nm diameter Mn-doped SnO<sub>2</sub> nanocrystals and nanowires. *Appl. Phys. Lett.* **2013**, *103*, 012401. [[CrossRef](#)]
71. Mounkachi, O.; El Moussaoui, H.; Masrour, R.; Ilali, J.; Mediouri, K.E.; Hamedoun, M.; Hlil, E.; El Kenz, A.; Benyoussef, A. High freezing temperature in SnO<sub>2</sub> based diluted magnetic semiconductor. *Mater. Lett.* **2014**, *126*, 193–196. [[CrossRef](#)]
72. Mehraj, S.; Ansari, M.S. Annealed SnO<sub>2</sub> thin films: Structural, electrical and their magnetic properties. *Thin Solid Film.* **2015**, *589*, 57–65. [[CrossRef](#)]
73. Wu, P.; Zhou, B.; Zhou, W. Room-temperature ferromagnetism in epitaxial Mg-doped SnO<sub>2</sub> thin films. *Appl. Phys. Lett.* **2012**, *100*, 182405. [[CrossRef](#)]
74. Mazloom, J.; Ghodsi, F.; Golmojdeh, H. Synthesis and characterization of vanadium doped SnO<sub>2</sub> diluted magnetic semiconductor nanoparticles with enhanced photocatalytic activities. *J. Alloy. Compd.* **2015**, *639*, 393–399. [[CrossRef](#)]
75. Chi, J.; Ge, H.; Wang, J.; Zuo, Y.; Zhang, L. Synthesis and electrical and magnetic properties of Mn-doped SnO<sub>2</sub> nanowires. *J. Appl. Phys.* **2011**, *110*, 083907. [[CrossRef](#)]

76. Liu, X.; Iqbal, J.; Wu, Z.; He, B.; Yu, R. Structure and room-temperature ferromagnetism of Zn-doped SnO<sub>2</sub> nanorods prepared by solvothermal method. *J. Phys. Chem. C* **2010**, *114*, 4790–4796. [[CrossRef](#)]
77. Zhi-Yuan, C.; Zhi-Quan, C.; Rui-Kun, P.; Shao-Jie, W. Vacancy-induced ferromagnetism in SnO<sub>2</sub> nanocrystals: A positron annihilation study. *Chin. Phys. Lett.* **2013**, *30*, 027804. [[CrossRef](#)]
78. Zhou, W.; Tang, X.; Xing, P.; Liu, W.; Wu, P. Possible room-temperature ferromagnetism in SnO<sub>2</sub> nanocrystalline powders with nonmagnetic K doping. *Phys. Lett. A* **2012**, *376*, 203–206. [[CrossRef](#)]
79. Hoa Hong, N.; Song, J.-H.; Raghavender, A.; Asaeda, T.; Kurisu, M. Ferromagnetism in C-doped SnO<sub>2</sub> thin films. *Appl. Phys. Lett.* **2011**, *99*, 052505. [[CrossRef](#)]
80. Zhang, L.; Ge, S.; Zuo, Y.; Wang, J.; Qi, J. Ferromagnetic properties in undoped and Cr-doped SnO<sub>2</sub> nanowires. *Scr. Mater.* **2010**, *63*, 953–956. [[CrossRef](#)]
81. Zima, T.; Bulina, N. Enhanced room-temperature ferromagnetism of Co-doped SnO<sub>2</sub> nanostructures produced by the hydrothermal method. *Mater. Res. Bull.* **2019**, *117*, 48–55. [[CrossRef](#)]
82. Mustaqima, M.; Liu, C. ZnO-based nanostructures for diluted magnetic semiconductor. *Turk. J. Phys.* **2014**, *38*, 429–441. [[CrossRef](#)]
83. Sun, Y.; Zong, Y.; Feng, J.; Li, X.; Yan, F.; Lan, Y.; Zhang, L.; Ren, Z.; Zheng, X. Oxygen vacancies driven size-dependent room temperature ferromagnetism in well-dispersed dopant-free ZnO nanoparticles and density functional theory calculation. *J. Alloy. Compd.* **2018**, *739*, 1080–1088. [[CrossRef](#)]
84. Qi, B.; Ólafsson, S.; Gíslason, H.P. Vacancy defect-induced room temperature ferromagnetism in undoped ZnO nanostructures: Controversial origin and challenges. *Prog. Mater. Sci.* **2017**, *90*, 45–74. [[CrossRef](#)]
85. Hagemark, K. Defect structure of Zn-doped ZnO. *J. Solid State Chem.* **1976**, *16*, 293–299. [[CrossRef](#)]
86. Hagemark, K.; Chacka, L. Electrical transport properties of Zn doped ZnO. *J. Solid State Chem.* **1975**, *15*, 261–270. [[CrossRef](#)]
87. Verma, A.; Tripathi, S. Magnetic annealing temperature modulated room temperature ferromagnetism in Zn doped ZnO thin film. *J. Magn. Magn. Mater.* **2019**, *478*, 28–37. [[CrossRef](#)]
88. Dietl, T.; Ohno, H.; Matsukura, F.; Cibert, J.; Ferrand, E.D. Zener model description of ferromagnetism in zinc-blende magnetic semiconductors. *Science* **2000**, *287*, 1019–1022. [[CrossRef](#)] [[PubMed](#)]
89. Seshadri, R. Zinc oxide-based diluted magnetic semiconductors. *Curr. Opin. Solid State Mater. Sci.* **2005**, *9*, 1–7. [[CrossRef](#)]
90. Sharma, D.K.; Sharma, K.K.; Kumar, V.; Sharma, A. Synthesis of Er doped ZnO cone-like nanostructures with enhanced structural, optical and magnetic properties. *J. Mater. Sci. Mater. Electron.* **2018**, *29*, 3840–3849. [[CrossRef](#)]
91. Valentin, C.B.S.; e Silva, R.L.D.S.; Banerjee, P.; Franco, A., Jr. Investigation of Fe-doped room temperature dilute magnetic ZnO semiconductors. *Mater. Sci. Semicond. Process.* **2019**, *96*, 122–126. [[CrossRef](#)]
92. Elilarassi, R.; Chandrasekaran, G. Optical, electrical and ferromagnetic studies of ZnO: Fe diluted magnetic semiconductor nanoparticles for spintronic applications. *Spectrochim. Acta Part A: Mol. Biomol. Spectrosc.* **2017**, *186*, 120–131. [[CrossRef](#)]
93. Torquato, R.; Shirsath, S.; Kiminami, R.; Costa, A. Synthesis and structural, magnetic characterization of nanocrystalline Zn<sub>1-x</sub>CoxO diluted magnetic semiconductors (DMS) synthesized by combustion reaction. *Ceram. Int.* **2018**, *44*, 4126–4131. [[CrossRef](#)]
94. Valério, L.; Mamani, N.; De Zevallos, A.; Mesquita, A.; Bernardi, M.; Doriguetto, A.; De Carvalho, H. Preparation and structural-optical characterization of dip-coated nanostructured Co-doped ZnO dilute magnetic oxide thin films. *RSC Adv.* **2017**, *7*, 20611–20619. [[CrossRef](#)]
95. Kayani, Z.N.; Nazir, F.; Riaz, S.; Naseem, S. Structural, optical and magnetic properties of manganese zinc oxide thin films prepared by sol-gel dip coating method. *Superlattices Microstruct.* **2015**, *82*, 472–482. [[CrossRef](#)]
96. Murmu, P.P.; Kennedy, J.; Ruck, B.J.; Rubanov, S. Microstructural, electrical and magnetic properties of erbium doped zinc oxide single crystals. *Electronic Mater. Lett.* **2015**, *11*, 998–1002. [[CrossRef](#)]
97. Aggarwal, N.; Vasishth, A.; Singh, B.; Singh, B. Investigation of room temperature ferromagnetic behaviour in dilute magnetic oxides. *Integr. Ferroelectr.* **2018**, *186*, 10–16. [[CrossRef](#)]
98. Das, A.; Sahoo, R.K.; Mishra, D.K.; Singh, S.K.; Mane, R.S.; Kim, K.H. Thermal plasma-inspired synthesis of ZnO<sub>1-x</sub>Mnx diluted magnetic semiconductors for enhanced visible light photocatalysis. *Appl. Surf. Sci.* **2019**, *467*, 1059–1069. [[CrossRef](#)]

99. Zargar, R.A.; Arora, M.; Bhat, R.A. Study of nanosized copper-doped ZnO dilute magnetic semiconductor thick films for spintronic device applications. *Appl. Phys. A* **2018**, *124*, 36. [[CrossRef](#)]
100. Tien, L.-C.; Hsieh, Y.-Y. Defect-induced ferromagnetism in undoped In<sub>2</sub>O<sub>3</sub> nanowires. *Mater. Res. Bull.* **2014**, *60*, 690–694. [[CrossRef](#)]
101. Sun, S.; Wu, P.; Xing, P. d<sub>0</sub> ferromagnetism in undoped n and p-type In<sub>2</sub>O<sub>3</sub> films. *Appl. Phys. Lett.* **2012**, *101*, 132417. [[CrossRef](#)]
102. Hong, N.H.; Sakai, J.; Huong, N.T.; Ruyter, A.; Brizé, V. Magnetism in transition-metal-doped In<sub>2</sub>O<sub>3</sub> thin films. *J. Phys. Condens. Matter* **2006**, *18*, 6897. [[CrossRef](#)]
103. Carvalho, M.; Piton, M.R.; Lemine, O.; Bououdina, M.; Galeti, H.V.A.; Souto, S.; Pereira, E.; Gobato, Y.G.; de Oliveira, A. Effects of strain, defects and crystal phase transition in mechanically milled nanocrystalline In<sub>2</sub>O<sub>3</sub> powder. *Mater. Res. Express* **2018**, *6*, 025017. [[CrossRef](#)]
104. An, Y.; Xing, Y.; Pan, F.; Wu, Z.; Liu, J. Investigation of local structural environments and room-temperature ferromagnetism in (Fe, Cu)-codoped In<sub>2</sub>O<sub>3</sub> diluted magnetic oxide films. *Phys. Chem. Chem. Phys.* **2016**, *18*, 13701–13709. [[CrossRef](#)] [[PubMed](#)]
105. Baqiah, H.; Ibrahim, N.; Halim, S.; Talib, Z.; Flaifel, M.; Abdi, M. Conducting mechanisms and magnetic behaviours of Fe-doped In<sub>2</sub>O<sub>3</sub> nanocrystalline films. *Results Phys.* **2017**, *7*, 1115–1121. [[CrossRef](#)]
106. Baqiah, H.; Ibrahim, N.; Halim, S.; Chen, S.; Lim, K.; Kechik, M.A. Physical properties of Fe doped In<sub>2</sub>O<sub>3</sub> magnetic semiconductor annealed in hydrogen at different temperature. *J. Magn. Magn. Mater.* **2016**, *401*, 102–107. [[CrossRef](#)]
107. Luo, X.; Tseng, L.-T.; Wang, Y.; Bao, N.; Lu, Z.; Ding, X.; Zheng, R.; Du, Y.; Huang, K.; Shu, L. Intrinsic or Interface Clustering-Induced Ferromagnetism in Fe-Doped In<sub>2</sub>O<sub>3</sub>-Diluted Magnetic Semiconductors. *ACS Appl. Mater. Interfaces* **2018**, *10*, 22372–22380. [[CrossRef](#)]
108. Garnet, N.S.; Ghodsi, V.; Hutflus, L.N.; Yin, P.; Hegde, M.; Radovanovic, P.V. Probing the role of dopant oxidation state in the magnetism of diluted magnetic oxides using Fe-doped In<sub>2</sub>O<sub>3</sub> and SnO<sub>2</sub> nanocrystals. *J. Phys. Chem. C* **2017**, *121*, 1918–1927. [[CrossRef](#)]
109. Krishna, N.S.; Kaleemulla, S.; Amarendra, G.; Rao, N.M.; Krishnamoorthi, C.; Kuppan, M.; Begam, M.R.; Reddy, D.S.; Omkaram, I. Structural, optical, and magnetic properties of Fe doped In<sub>2</sub>O<sub>3</sub> powders. *Mater. Res. Bull.* **2015**, *61*, 486–491. [[CrossRef](#)]
110. Peleckis, G.; Wang, X.; Dou, S. Ferromagnetism in Mn-doped In<sub>2</sub>O<sub>3</sub> oxide. *J. Magn. Magn. Mater.* **2006**, *301*, 308–311. [[CrossRef](#)]
111. Pellicer, E.; Menéndez, E.; Fornell, J.; Nogués, J.; Vantomme, A.; Temst, K.; Sort, J. Mesoporous oxide-diluted magnetic semiconductors prepared by Co implantation in nanocast 3D-ordered In<sub>2</sub>O<sub>3-y</sub> materials. *J. Phys. Chem. C* **2013**, *117*, 17084–17091. [[CrossRef](#)]
112. Kumagai, H.; Hara, Y.; Sato, K. Site occupancy, valence state, and spin state of Co ions in Co-doped In<sub>2</sub>O<sub>3</sub> diluted magnetic semiconductor. *J. Magn. Magn. Mater.* **2019**, 165358. [[CrossRef](#)]
113. Shen, L.; An, Y.; Cao, D.; Wu, Z.; Liu, J. Room-Temperature Ferromagnetic Enhancement and Crossover of Negative to Positive Magnetoresistance in N-Doped In<sub>2</sub>O<sub>3</sub> Films. *J. Phys. Chem. C* **2017**, *121*, 26499–26506. [[CrossRef](#)]
114. Cao, H.; Xing, P.; Zhou, W.; Yao, D.; Wu, P. Indium vacancy induced d<sub>0</sub> ferromagnetism in Li-doped In<sub>2</sub>O<sub>3</sub> nanoparticles. *J. Magn. Magn. Mater.* **2018**, *451*, 609–613. [[CrossRef](#)]

